G

Geochemistry of Sublacustrine Hydrothermal Deposits in Yellowstone Lake—Hydrothermal Reactions, Stable-Isotope Systematics, Sinter Deposition, and Spire Formation

By Wayne C. Shanks, III, Jeffrey C. Alt, and Lisa A. Morgan

Chapter G *of*
Integrated Geoscience Studies in the Greater Yellowstone Area—Volcanic, Tectonic, and Hydrothermal Processes in the Yellowstone Geoecosystem
Edited by Lisa A. Morgan

U.S. Geological Survey Professional Paper 1717

U.S. Department of the Interior
U.S. Geological Survey

Contents

Figures

Tables

Geochemistry of Sublacustrine Hydrothermal Deposits in Yellowstone Lake—Hydrothermal Reactions, Stable-Isotope Systematics, Sinter Deposition, and Spire Formation

By Wayne C. Shanks, III,[1] Jeffrey C. Alt,[2] and Lisa A. Morgan[1]

Abstract

Geochemical and mineralogical studies of hydrothermal deposits and altered vent muds from the floor of Yellowstone Lake indicate that these features form due to hydrothermal fluid quenching in shallow flow conduits or upon egress into bottom waters. Siliceous precipitates occur as conduits within the uppermost sediments, as tabular deposits that form along sedimentary layers, and as spires as much as 8 m tall that grow upward from crater-like depressions on the lake bottom. These deposits are enriched in As, Cs, Hg, Mo, Sb, Tl, and W.

Variations in major-element geochemistry indicate that subaerial sinters from West Thumb and spire interiors are nearly pure SiO_2, whereas sublacustrine conduits are less SiO_2 rich and are similar in some cases to normal Yellowstone Lake sediments due to incorporation of sediments into conduit walls. Vent muds, which are hydrothermally altered lake sediments, and some outer conduit walls show pervasive leaching of silica (~63 weight percent silica removal). This hydrothermal leaching process may explain the occurrence of most sublacustrine vents in holes or vent craters, but sediment winnowing by vent fluids may also be an important process in some cases.

Stable-isotope studies indicate that most deposits formed at temperatures between 78°C and 160°C and that vent fluids had oxygen-isotope values of –3.2 to –11.6 per mil, significantly higher than lake waters (–*16.5 per mil). Sulfur-isotope studies indicate that vent waters and lake waters are dominated by sulfur derived from volcanic rocks with $\delta^{34}S$ ~ 2.5 per mil.

Geochemical reaction modeling indicates that spires form from upwelling hydrothermal fluids that are saturated with amorphous silica at temperatures 80°–96°C. Reaction calculations suggest that silica precipitation on the lake bottom is initially caused by mixing with cold bottom waters. Once a siliceous carapace is established, more rapid silica precipitation occurs by conductive cooling. Silicification of thermophilic bacteria is a very important process in building spire structures.

Introduction

Yellowstone Lake at 2,356 m altitude is the largest high-altitude lake in North America and is an important scenic attraction and pristine environment in America's first National Park. Famous for abundant and spectacular hydrothermal activity, Yellowstone National Park (the Park) is home to hundreds of geysers, boiling pools, terraces, and acid-steam environments—and thus results from recent high-resolution bathymetric and seismic mapping that indicate hundreds of hydrothermal vents on the lake floor generally are consistent with distributions of thermal features in major subaerial geyser basins (Morgan and others, 2003).

Studies of hydrothermal vent fluids in Yellowstone Lake have shown that a number of elements, including B, Li, Cs, Cl, As, Sb, Hg, Mo, and W, are strongly enriched in vent fluids and in the lake water column due to hydrothermal venting (Balistrieri and others, this volume; Gemery-Hill and others, this volume). Moreover, these studies, combined with Park-wide studies of Cl fluxes in streams (Friedman and Norton, this volume), indicate that 10 percent of the flux of deep hydrothermal water in Yellowstone National Park occurs on the Yellowstone Lake bottom as sublacustrine hydrothermal vents (Balistrieri and others, this volume). The sublacustrine vents and associated deposits represent several of the most important thermal fields in Yellowstone National Park, comparable in size and hydrothermal flux to Norris Geyser Basin or the Old Faithful area.

Yellowstone Lake also holds a unique position in the geoecosytem of the Park; the native and threatened cutthroat trout in the lake are particularly important because they spawn in the rivers and are important food sources for otter, bear, and eagles. Indeed, geochemical studies of trace metals and stable isotopes show that mercury in sublacustrine hydrothermal vents is incorporated into cutthroat trout and occurs as significantly elevated mercury content in the hair of bears that feed near Yellowstone Lake (Chaffee, Shanks, and others, this volume, Felliceti and others, 2004).

[1]U.S. Geological Survey, Box 25046, Mail Stop 973, Denver Federal Center, Denver, CO 80225.

[2]Department of Geological Sciences, C.C. Little Building, The University of Michigan, Ann Arbor, MI 48109.

In this report, we document the occurrence of sublacustrine hydrothermal deposits and their mineralogy, chemistry, and stable-isotope composition in order to understand their origins and implications for processes involving hydrothermal fluids venting on the lake bottom.

Geologic Setting

Yellowstone National Park occupies a region of young and active tectonism and volcanism related to its current position over a deep long-lived thermal disturbance (Humphreys and others, 2000; Christiansen and others, 2002) refered to as the Yellowstone hotspot (Pierce and Morgan, 1992; Smith and Braile, 1994). Migration of the North American plate over the Yellowstone hotspot beginning at ~16 Ma has produced a progression of silicic volcanic fields containing nested caldera complexes along the Snake River Plain (Pierce and Morgan, 1992). This track of silicic magmatism is exposed along the margins of and reflected in the topographically low Snake River Plain (Armstrong and others, 1975; Morgan and others, 1984; Perkins and Nash, 2002; Kellogg and others, 1994; Morgan, 1992; Leeman, 1982; Hughes and McCurry, 2002; Bonnichsen, 1982); the hotspot is now centered on the topographically high Yellowstone Plateau (Pierce and Morgan, 1992; Pierce and others, this volume).

Large-volume, high-silica rhyolitic ignimbrites and lava flows have erupted from overlapping and nested calderas in the Yellowstone Plateau volcanic field producing an estimated total eruptive volume of 3,700 km^3 (Christiansen, 2001). Major caldera-forming eruptions occurred at 2.05 Ma, 1.3 Ma, and 0.64 Ma (Christiansen, 2001). The 0.64-Ma Yellowstone caldera is the locus of most active hydrothermal activity in the Park. Seismic studies (Christiansen, 2001; Miller and Smith, 1999) suggest that a zone of magma below the caldera, at about 5–6 km deep, fuels the hydrothermal activity of Yellowstone National Park. Further, Fournier (1999) argues that the hydrothermal fluids circulate above the depth of brittle-ductile transition depth (3–5 km) and that there may be periodic exchange of magma or brine across this interface.

Yellowstone Lake straddles the southeastern topographic margin of the 0.64-Ma Yellowstone caldera (fig. 1), resulting in the northern two-thirds of the lake lying within the caldera and containing most of the sublacustrine hydrothermal activity. The eastern boundary of the northern part of the lake corresponds with the eastern edge of the Yellowstone caldera (Morgan and others, 2003). Mary Bay, a large scalloped embayment on the northern edge of the lake, formed around 13,600 years ago as a series of sublacustrine hydrothermal-explosion events (Wold and others, 1977; Morgan and others, 1998; Pierce and others, 2002). West Thumb basin, in the western reaches of Yellowstone Lake, formed during eruption of the ~140-ka tuff of Bluff Point (Obradovich, 1992) and subsequent collapse of the West Thumb caldera (Christiansen, 2001).

Hydrothermal vent areas in Yellowstone Lake have been known since the first surveys of the area in the late 1800s (Hayden, 1878). Bathymetric and additional geophysical surveys conducted by Wold and others (1977), Otis (1975), Otis and others (1977), and Kaplinski (1991) and vent sampling by the University of Wisconsin-Milwaukee (Klump and others, 1988; Remsen and others, 1990) better established the existence and location of several hydrothermal vent fields within the lake. These studies clearly show that abundant sublacustrine hydrothermal activity occurs within the Yellowstone caldera (fig. 1). West Thumb basin and the northern basin (fig. 1) related to exceptionally high heat flow (Morgan and others, 1977). The South and Southeast Arms of the lake, well outside the caldera boundary, are of glacial origin and exhibit little evidence of hydrothermal activity.

More recently, USGS high-resolution bathymetric mapping of Yellowstone Lake from 1999–2002 has identified more than 300 hydrothermal vents on the lake floor, mainly in the West Thumb and northern basins but also in the central basin (Morgan and others, 2003; Morgan and others, this volume). Exploration, photographic documentation, and sampling with a submersible remotely operated vehicle (ROV) has revealed different types of hydrothermal deposits on the lake bottom, including siliceous conduits formed due to hydrothermal fluid flow through surficial sediments in areas of active or previously active venting and a spectacular group of 12–15 spires of siliceous sinter as much as 8 m tall. Siliceous sinter deposits in Yellowstone Lake are of broad interest because they may be analogous to some important ancient mineral deposits that are hosted by siliceous sinter in lake beds (Cunneen and Sillitoe, 1989; Ebert and Rye, 1997). Similar small sublacustrine sinter deposits have been reported from Lake Taupo, New Zealand (de Ronde and others, 2002). Inactive siliceous spires have been observed in one area in Crater Lake, Oregon (Robert Collier, Oregon State University, written commun.; Bacon and others, 2002), but they have not been studied in detail.

Acknowledgments

This work could not have been done without the support of the National Park Service, especially Mike Finley, John Varley, Tom Olliff, Paul Doss, Dan Reinhart, Rick Fey, John Lounsbury, Dan Mahoney, Jim Ruzycki, Todd Koel, and the Aquatic Resources Group at Lake Station. We are particularly indebted to Dave Lovalvo of Eastern Oceanics, Inc., who designed, built, and piloted the ROV and the research vessel (R.V. *Cutthroat*) and generously shared his incredible knowledge of Yellowstone Lake. We thank Kate Johnson, Ed du Bray, Geoff Plumlee, Pat Leahy, Steve Bohlen, Tom Casadevall, Linda Gundersen, Denny Fenn, Elliott Spiker, and Dick Jachowski for supporting this work. We thank Dan Reinhart, Paul Doss, Ann Deutch, Christie Hendrix, Pam Gemery-Hill, Rick Sanzolone, Al Meier, Pete Theodorakos, Jim Bruckner, Bree Burdick, Steve Harlan, Greg Meeker, Jim Waples, Bob Evanoff, Wes Miles, Rick Mossman, Gary Nelson, Eric White, and many others for assistance with field and laboratory studies. We especially

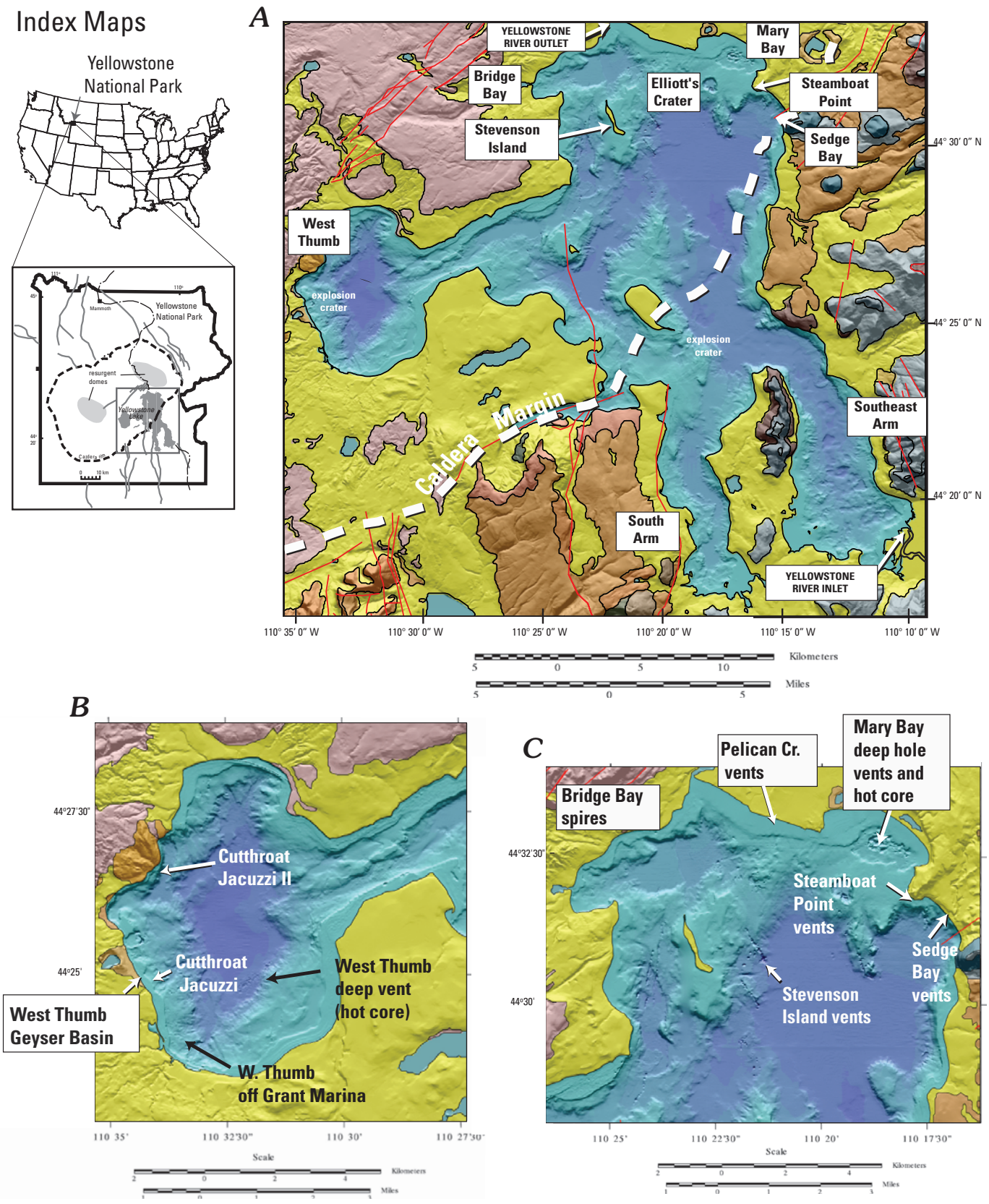

Figure 1. *A,* Bathymetric map of Yellowstone Lake. *B,* Detailed bathymetric map of West Thumb showing locations of hydrothermal sites. *C,* Detailed bathymetric map of northern Yellowstone Lake showing locations of hydrothermal sites.

Table 1. Mineralogy of vent deposits and vent muds from X-ray diffraction (XRD) and scanning electron microscopy.

[Co, conduit; Cr, crust; Sed, sediment; Ab, albite; Sm, smectite; Vill, villyaellenite—a Mn-As oxyhydroxide: $(MnCaZn)_5(AsO_3OH)_2(AsO_4)_2.4(H_2O)$—Am, amorphous; Gt, goethite; Interst, interstitial; Am Si, amorphous silica]

Sample	Type	Description	XRD			Location
			Major	Minor	Trace	
		Vent deposits				
BS 8	co	~3-cm-diameter conduit; porous gray, hard gray, soft buff	Qz, Ab, Opal		Ill, Sm	Mary Bay
			Opal	Qz, Ab	Sm, Ill	Mary Bay
			Opal		Qz, Ab	Mary Bay
94-7-1(D-7)	cr	Irregular gray "crust" and conduits; composed of lithified sediment				Mary Bay
94-11-2	co	1- to 2-cm-diameter conduits; gray inner, buff outer; porous white and red-brown precipitates	Qz, Ab, Opal;	Sm, Illite		Mary Bay
			Opal	Qz, Ab	Sm, Ill	Mary Bay
			Opal			Mary Bay
94-12-2	co	3- to 4-cm-diameter conduit; harder inner and softer outer layers; composed of lithified sediment?	Qz, Ab	Opal	Sm, Ill, Gyp	Mary Bay
94-12-4	cr	Soft, buff-colored "crust" composed of semilithified sediment?				Mary Bay
94-13-2	co	1-cm-diameter white-buff conduit; hard gray-brown lining; sedimentary layering?				Mary Bay
94-23-1	cr	1- to 2.5-cm-thick "crust;" harder gray core (lithified sediment?); red-brown stains				Mary Bay
94-24-2 tube	co	2.5-cm-diameter conduit; white, hard gray, soft buff				Mary Bay
94-24-2 crust	cr	1–2 cm thick; irregular, semilithified sediment; buff; 0.5-mm-diameter holes	Qz, Ab	Opal	Sm, Ill	Mary Bay
94-?	co+cr	2-cm-diameter conduit and crust with sediment (conduit?); all are buff; lithified sediment?				Mary Bay
98-3	cond	~15-cm-long double conduit; stained by iron oxide				Mary Bay
98-11	co	3- to 4-cm-diameter conduit; 1.5 cm internal diameter; 0.5–2 cm wall (7×10-inch relict conduit)				Mary Bay
	cr	1- by 3- to 5-cm-crust fragments (7×10-inch relict conduit, inverted mushroom)				Mary Bay
YNP 89 SBS-11	tubes	Aggregrate of 1 mm gray tubes; lt gray sed interst; pyrite	Pyrite		Vill>Qz, Ab, Sm, Ill	Sedge Bay
94-14-1 Stv Is	co/cr	Irregular conduit?; hard gray, softer gray, yellow coat; tiny crystal rosettes	Na-Jarosite, Gyp		Qz, Ab, Opal	Stevenson Island
94-14-4	co	1.5 cm buff-orange conduits; hard brown silica lining				Stevenson Island
97 WTGB	sinter	Chunk of subaerial sinter	Opal only			West Thumb Geyser Basin
98-16 cond	co	19-inch-long conduit; 2–10 mm walls; brown iron oxide coating, mud fill	Qz	Opal	Sm, Ill	W Thumb, off marina
98-17 cond	co	12-inch-long relict conduit; sediment ridges; 2-inch-diameter and 3-mm-thick wall				W Thumb, off marina
98-18 crust	cr	10×13-inch crust (vein in sed?); 3 mm–3 cm thick; variably silicified; brown FeMn oxide stain				W Thumb, off marina
98-18 sntr	sinter	1×2-inch fragment of white sinter/crust (similar to above sample?)				W Thumb, off marina
98-21	co	6×8-inch mushroom conduit; section through neck; Am Si, native S; mud	Opal		Qz, Ab, Sm	W Thumb, deep
			Opal		Qz, Ab, Sm	
			Opal		Qz, Ab, Ill	
98-22	co	Double conduit; section through throat, tip of neck, and soft outer mud				W Thumb, deep

Table 1. Mineralogy of vent deposits and vent muds from X-ray diffraction (XRD) and scanning electron microscopy—*Continued*.

Sample	Type	Description	XRD			Location
			Major	Minor	Trace	
98-23D-A	co	4×6.5-inch conduit; 2-cm-diameter neck; iron oxide stained; hard 2–3 cm fragments at base; sediment and silica veins				W Thumb, deep
98-24	co	9×10-inch relict conduit with lacy network of tubes; 1-inch-diameter irregular center conduit stained and cemented by red-brown iron oxide				W Thumb, deep
		Bridge Bay spires				
97 BB-1	spire	Chunk of spire	Opal		Ab, Sm, Ill	Bridge Bay spire
	spire	Outer surface	Opal, Am. FeOx		Gt (broad pks)	Bridge Bay spire
97 BB-2	spire	Chunk of spire	Opal only			Bridge Bay spire
		Vent muds				
98-3	mud	Associated with conduit; olive green mud				Mary Bay
98 core 3	mud	1: 0–10 cm long; dark green-black mud; hot (~50 cm core)	Qz, Ab	Sm	Gyp, Ill	Mary Bay
98 core 3	mud	2: 20–30 cm long; dark green-black mud; hot	Qz, Ab	Gyp	Sm, Ill	Mary Bay
98 core 3	mud	3: 40–45 cm long; dark green-black mud; hot	Qz, Ab	Gyp	Ill	Mary Bay
98-26	mud	Dark olive brown mud around active 60°C vent	Qz, Ab	Ill, Sm		Mary Bay
98-27	sed	Dark olive brown mud and consolidated sediments at active 103°C vent	Qz, Ab, Sm	Gyp	Illite	Mary Bay
98-SB 0-1cm	sand	Brown sand; diver core over active vent/bubbler				Sedge Bay
98-SB 5-6 cm	sand	Gray sand				Sedge Bay
98-29	mud	Dark olive brown mud at active vent				E of Stevenson Is
98-29	sed	Gray-black consolidated mud; 1–3 cm clasts				E of Stevenson Is
98-29	sulfide	Pyrite and native S veins and blobs				E of Stevenson Is
98-30	mud	Gray mud from edge of large inactive hole (1–2 ft diameter)	Chl	Sm	Qz, Ab, Ill	E of Stevenson Is
98-32	mud	Mud from around active vents	Chl, Qz	Sm, Ab	Ill	E of Stevenson Is
98-16 in mud	mud	Mud inside conduit; brown-buff				W Thumb, off marina
98-16 out mud	mud	Mud outside conduit; when wet is dark green-brown				W Thumb, off marina
98-17 sedmnt	sed	Consolidated green mud with black FeMn oxide veins and coatings				W Thumb, off marina
98-19	sed	Consolidated gray sediment; stained red-brown by iron oxide	Qz	Chl	Ab, Ill	W Thumb, deep
98-20	sed	Green-gray lithified sediment; angular coarse sandstone and obsidian fragments				W Thumb, deep
		Unaltered West Thumb sediment				
WT89 sediment core	sed	25–26 cm long; tan sediment	Opal		Ab, Qz, Illite, Sm	West Thumb
WT89 sediment core	sed	26–27 cm long; tan sediment	Opal		Ab, Qz, Illite, Sm	West Thumb

thank Greg Lee and Mike Webring of the USGS for turning raw data into beautiful maps. We thank Val Klump, Russell Cuhel, Tony Remsen, and Carmen Aguilar of the University of Wisconsin-Milwaukee for introducing us to Yellowstone Lake vent studies and for sharing samples. Marty Goldhaber and Rich Wanty provided constructive reviews that substantially improved the manuscript. This research was supported by the U.S. Geological Survey, the National Park Service, the National Science Foundation (Environmental Geochemistry and Biogeochemistry), and the Yellowstone Foundation.

Methods

Representative samples of siliceous hydrothermal deposits and sediments were collected from the lake bottom in conjunction with hydrothermal-water-sampling operations (Balistrieri and others, this volume). Most samples were collected with a submersible remotely operated vehicle (ROV) designed and piloted by Dave Lovalvo of Eastern Oceanics, Inc. Although the exact configuration of the vehicle varied from year to year, it was equipped with a motorized scoop for collecting solid samples by remotely maneuvering the submersible while making video observations in the control room of the support boat. Some sediment samples were collected by gravity coring.

Minerals were characterized by X-ray diffraction (XRD) analysis, performed on sample powders using an automated Scintag diffractometer with Cu kα radiation. Samples also were examined by scanning electron microscopy (SEM), using a HITACHI S-3200N SEM, equipped with a Noran X-ray energy-dispersive system (EDS). Mineralogy of samples is summarized in table 1.

Samples were crushed and ground to <200 mesh for chemical analyses. All chemical and isotopic analyses were done in the USGS laboratories in Denver, Colo. Major-element analyses were carried out on fused pellets by wavelength-dispersive X-ray fluorescence (table 2). Forty trace and minor elements were analyzed by inductively coupled plasma–mass spectrometry (ICP–MS) following sample dissolution in HNO_3-HF solution. Mercury was analyzed on separate acid dissolutions using flameless atomic absorption (AA) analysis. Trace- and minor-element data are summarized in table 3.

Silicate samples for oxygen-isotope analysis were reacted with BrF_5 in nickel reaction vessels (Clayton and Mayeda, 1963) to liberate O_2, which was converted to CO_2. Oxygen-isotope values ($\delta^{18}O$) were analyzed on a Finnigan 252 isotope ratio mass spectrometer and calibrated relative to the VSMOW (Vienna Standard Mean Ocean Water; Coplen, 1995) standard with reproducibility of approximately 0.2 per mil. Sulfur-bearing phases were analyzed for $\delta^{34}S$ using an automated elemental analyzer interfaced to a Micromass Optima isotope ratio mass spectrometer (Giesemann and others, 1994). $\delta^{34}S$ error is estimated to be 0.2 per mil. Stable-isotope data are included in table 2.

Occurrence and Mineralogy of Hydrothermal Deposits in Yellowstone Lake

Active hydrothermal vents and associated vent deposits have been observed at many locations in Yellowstone Lake (fig. 1) including shallow-water vents in nearshore locations in West Thumb, Mary Bay, off Steamboat Point, and in Sedge Bay; moderate-depth (25–50 m) vents in West Thumb basin and in the Mary Bay hydrothermal-explosion-crater complex; and in the deepest part of the lake (95–110 m) off Stevenson Island

Large hydrothermal-explosion craters (>500-m diameter) are known in subaerial hydrothermal areas in Yellowstone National Park and elsewhere (Browne and Lawless, 2001; Morgan, Shanks, and others, 1998; Muffler and others, 1971). High-resolution bathymetric surveys in recent years have identified a number of large hydrothermal-explosion craters on the lake floor (Morgan and others, this volume; Morgan and others, 2003). These include the Mary Bay crater complex, a large crater southeast of Storm Point informally named Elliott's Crater (Morgan and others, 2003; Morgan and others, this volume; Johnson and others, 2003), a nearshore crater in West Thumb north of West Thumb Geyser Basin, and a crater south of the caldera margin in the central lake (fig. 1). Hydrothermal activity has been observed in many of these explosion craters, and additional data on related vent fluids is presented in Gemery-Hill and others (this volume).

High-resolution bathymetric mapping has located more than 650 vent craters in Yellowstone Lake (Morgan and others, this volume; Morgan and others, 2003). At sublacustrine vent sites, shimmering hydrothermal fluids, with or without bubbles, typically exit from small (~1–5 cm in diameter) vents within unconsolidated or semi-indurated sediment, at temperatures of ~10°–120°C. Most sublacustrine hydrothermal vents in Yellowstone Lake occur within localized bathymetric deeps or small craters, here called vent craters, which are most commonly ~1–10 m wide and ~10–20 m deeper than the surrounding lake floor. The largest of the vent craters is off the eastern shore of Stevenson Island (fig. 1*C*) and is about 220 m wide and 50 m deeper than the surrounding lake bottom (fig. 2). This structure is in the northernmost set of three northwest-trending fissures; its location is at the southeastern end of the line of vents (fig. 1). It contains numerous individual vents, as indicated by seismic reflection profiles across this structure (Johnson and others, 2003) and by photographic documentation with the ROV exploration and sampling of thermal fluids and solids.

Sediment is exposed in the walls of many of these vent craters, especially in West Thumb basin and off the eastern shore of Stevenson Island. Solid samples and submersible observations show that the sediments are laminated, semi-indurated, fractured, and jointed, breaking into angular centimeter- to decimeter-size blocks. Recent unconsolidated sedi-

Table 2. Major element and stable-isotope data for vent deposits and vent muds.

[Chemical analyses by wavelength-dispersive X-ray fluorescence (WD-XRF) and by inductively coupled plasma–mass spectrometry (ICP-MS). LOI, loss on ignition]

Sample number/description	Location	$\delta^{34}S$	$\delta^{18}O$	SiO_2* (wt %)	Al_2O_3 (wt %)	CaO (wt %)	$FeTO_3$ (wt %)	K_2O (wt %)	MgO (wt %)	MnO (wt %)	Na_2O (wt %)	P_2O_5 (wt %)	TiO_2 (wt %)	S (wt %)	LOI (925°C)	Total	Analytical method
98-11, MB relict conduit	Mary Bay			76.4	7.54	1.8	2.26	1.14	0.7	0.02	1.27	0.18	0.3	0.12	7.2	98.9	WD-XRF
98-11, MB crust	Mary Bay			77.1	7.56	1.83	1.84	1.13	0.83	0.02	1.29	0.13	0.3	0.25	7.7	100.0	WD-XRF
94-11-2, MB bulk conduit	Mary Bay			84.1	5.10	0.84	1.30	0.73	0.40	0.023	0.71	0.27	0.17	0.20			ICP-MS
94-11-2, MB inner conduit	Mary Bay		8.6	87.4	2.83	0.56	1.22	0.42	0.25	0.008	0.49	0.14	0.13	0.40			ICP-MS
94-11-2, MB outer conduit	Mary Bay			80.1	7.18	1.20	1.86	1.11	0.50	0.046	1.15	0.37	0.33	< 0.1			ICP-MS
94-12-2, MB bulk conduit	Mary Bay			81.9	5.29	1.23	2.43	0.80	0.46	0.026	0.96	0.41	0.17	0.20			ICP-MS
94-12-4, MB crust	Mary Bay			74.5	9.83	2.38	2.14	1.45	0.93	0.039	1.75	0.37	0.50	< 0.1			ICP-MS
94-13-2, MB bulk conduit	Mary Bay			84.4	4.53	0.92	1.57	0.65	0.41	0.046	0.67	0.37	0.17	0.10			ICP-MS
94-13-2, MB inner conduit	Mary Bay		8.5	89.5	2.27	0.42	0.56	0.33	0.20	0.009	0.32	0.09	0.10	0.10			ICP-MS
94-13-2, MB outer conduit	Mary Bay			83.6	4.91	0.95	1.72	0.73	0.43	0.194	0.75	0.41	0.17	< 0.1			ICP-MS
94-14-4, MB outer conduit	Mary Bay			72.0	10.0	1.82	4.72	1.57	0.53	0.101	1.75	0.50	0.50	0.40			ICP-MS
94-23-1, MB bulk crust	Mary Bay			82.2	5.86	1.13	1.72	0.75	0.50	0.023	0.88	0.32	0.33	0.20			ICP-MS
94-23-1, MB inner crust	Mary Bay			84.5	4.35	1.09	1.43	0.60	0.51	0.022	0.75	0.27	0.17	0.20			ICP-MS
94-23-1, MB outer crust	Mary Bay			76.2	8.50	2.38	2.14	1.18	0.65	0.074	1.35	0.46	0.33	0.60			ICP-MS
94-24-2-A, MB crust	Mary Bay			77.2	7.75	1.96	2.57	1.14	0.90	0.058	1.48	0.50	0.33	< 0.1			ICP-MS
94-24-2-B, MB bulk conduit	Mary Bay		16.3	77.9	7.75	1.96	2.00	1.11	0.99	0.037	1.35	0.32	0.33	0.10			ICP-MS
94-3, MB bulk conduit	Mary Bay			81.2	6.05	1.54	1.57	0.92	0.63	0.101	1.13	0.23	0.33	0.20			ICP-MS
94-7-1, MB crust	Mary Bay			77.3	7.94	2.10	2.00	1.16	1.03	0.039	1.48	0.32	0.33	0.20			ICP-MS
BS8, MB bulk conduit	Mary Bay		9.8	83.0	6.05	0.85	1.20	0.86	0.32	0.018	0.86	0.23	0.33	0.20			ICP-MS
BS8, MB inner conduit	Mary Bay			88.0	2.83	0.56	0.79	0.42	0.25	0.007	0.47	0.09	0.13	0.30			ICP-MS
BS8, MB outer conduit	Mary Bay			82.3	6.05	0.95	1.43	0.94	0.38	0.022	0.98	0.27	0.33	0.20			ICP-MS
YNP-89-SBS-11, pyritic tubes w/ sediment	Sedge Bay			13.1	5.10		44.32	0.08	0.03	0.001		0.09	0.17	31.00			ICP-MS
98-29, SI sediment & pyrite veins	Stevenson Island													23			WD-XRF
94-14-1, SI bulk conduit	Stevenson Island			73.9	9.45	1.82	3.29	1.33	0.63	0.021	1.62	0.32	0.33	1.20			ICP-MS
94-14-1, SI inner conduit/crust	Stevenson Island		13.5	81.8	5.67	1.15	1.72	0.84	0.50	0.013	1.09	0.18	0.33	0.60			ICP-MS
94-14-1, SI outer conduit	Stevenson Island			75.4	8.50	1.82	2.86	1.20	0.66	0.019	1.62	0.32	0.33	1.10			ICP-MS
94-14-4, SI bulk conduit	Stevenson Island			68.6	12.3	2.10	4.86	1.81	0.65	0.046	2.02	0.50	0.50	0.50			ICP-MS
94-14-4, SI inner conduit	Stevenson Island			84.1	4.91	0.92	1.40	0.76	0.28	0.023	0.89	0.18	0.17	0.20			ICP-MS
98-22, WT double conduit	West Thumb deep vent			88.1	2.02	0.31	0.46	0.42	< 0.10	0.01	0.19	0.1	0.07		6.6	98.2	WD-XRF

Table 2. Major element and stable-isotope data for vent deposits and vent muds—*Continued*.

Sample number/description	Location	$\delta^{34}S$	$\delta^{18}O$	SiO_2* (wt %)	Al_2O_3 (wt %)	CaO (wt %)	$FeTO_3$ (wt %)	K_2O (wt %)	MgO (wt %)	MnO (wt %)	Na_2O (wt %)	P_2O_5 (wt %)	TiO_2 (wt %)	S (wt %)	LOI (925°C)	Total	Analytical method
98-23D, WT slab	West Thumb deep vent		17.1	91.1	0.60	0.08	0.33	0.15	< 0.10	< 0.01	< 0.15	0.08	0.04	0.08	5.9	98.3	WD-XRF
98-23d, WT conduit	West Thumb deep vent			93.6	0.72	0.09	0.32	0.17	< 0.10	0.03	< 0.15	0.09	0.04	b.d.	3.8	98.9	WD-XRF
98-24, WT relict, lacy conduit	West Thumb deep vent			81.0	2.87	0.45	3.26	0.34	0.17	1.91	0.19	0.29	0.09	b.d.	7.5	98.1	WD-XRF
98-16, WT conduit	West Thumb off Grant			78.8	6.64	0.7	2.37	1.85	0.23	0.95	1.22	0.28	0.23	b.d.	5.6	98.8	WD-XRF
98-18, WT sinter crust	West Thumb off Grant		20.3	91.1	1.09	0.16	0.73	0.22	< 0.10	0.48	< 0.15	0.08	0.05	b.d.	4.8	98.7	WD-XRF
BRIDGE BAY SPIRES																	
97-BB1, dark outer sinter	NE Bridge Bay		16.1	89.1	2.27	0.28	0.81	0.19	0.25	0.106	0.22	0.37	0.05	0.20			ICP-MS
97-BB1, white/tan inner sinter	NE Bridge Bay		13.7	83.3	6.42	0.81	1.19	0.60	0.53	0.010	0.70	0.18	0.15	<0.1			ICP-MS
97-BB2, dark outer sinter	NE Bridge Bay		8.0	73.3	8.31	1.33	7.43	0.72	0.68		0.77	0.96	0.17	0.20			ICP-MS
97-BB2, white/tan inner sinter	NE Bridge Bay		14.7	88.8	1.57	0.14	2.57	0.10	0.17	0.015	0.07	0.41		<0.2			ICP-MS
WEST THUMB SINTERS																	
97-WTGB-1, WT sinter	Sinter terrace WTGB		20.7	93.6	0.38	<0.07	0.04	0.09	<0.02	< 0.01	0.32	<0.05	<0.02	<0.1			ICP-MS
98P94-A, WT sinter	Fishing Cone, 4 ft deep		21.4	91.7	0.52	0.15	0.1	0.12	< 0.10	< 0.01	< 0.15	0.06	< 0.02		5.3	98.0	WD-XRF
98P94-B, WT sinter	Fishing Cone, 7 ft deep			92.0	0.50	0.1	0.1	0.11	< 0.10	< 0.01	< 0.15	0.06	0.030		5.9	98.8	WD-XRF
98P94-C, WT sinter	50m N of Fishing Cone, 4.5 ft deep			90.6	0.40	0.09	0.1	0.05	< 0.10	< 0.01	< 0.15	< 0.05	< 0.02		7.5	98.7	WD-XRF

Table 2. Major element and stable-isotope data for vent deposits and vent muds—*Continued* .

Sample number/description	Location	$\delta^{34}S$	$\delta^{18}O$	SiO_2* (wt %)	Al_2O_3 (wt %)	CaO (wt %)	$FeTO_3$ (wt %)	K_2O (wt %)	MgO (wt %)	MnO (wt %)	Na_2O (wt %)	P_2O_5 (wt %)	TiO_2 (wt %)	S (wt %)	LOI (925°C)	Total	Analytical method
WEST THUMB SINTERS—*Continued*																	
98P95-B, WT sinter	70 m off Fishing Cone, 14.5 ft deep		20.6	93.7	0.35	0.07	0.1	0.07	< 0.10	< 0.01	< 0.15	< 0.05	< 0.02		4.6	98.9	WD-XRF
98P96-B, WT sinter	70m/20 deg S of Fishing Cone, 18 ft deep			92.7	1.10	0.11	0.2	0.10	< 0.10	0.01	< 0.15	0.08	0.030		4.8	99.2	WD-XRF
VENT MUDS																	
98-03, vent mud	Mary Bay	4.6	8.8	67.2	14.7	2.80	3.57	2.05	1.34	0.027	2.16			0.0010			ICP-MS
98-26, vent mud	Mary Bay	0.7	8.4	65.6	14.7	2.94	4.43	1.93	2.16	0.043	2.02			0.03			ICP-MS
98-27, vent mud	Mary Bay	0.8	8.1	70.1	14.9	1.54	3.29	1.20	1.82	0.027	0.89			0.03			ICP-MS
Core 3-1 (0–10 cm), vent mud	Mary Bay	3.4	7.0	70.1	12.7	2.52	3.15	2.05	1.29	0.031	2.02			0.01			ICP-MS
Core 3-2 (20–30 cm), vent mud	Mary Bay	5.7	7.2	70.6	11.9	2.66	3.43	1.81	1.33	0.032	2.16			0.0020			ICP-MS
Core 3-3 (40–45 cm), vent mud	Mary Bay	3.7	8.3	68.8	12.8	2.80	3.72	1.93	1.66	0.039	2.02			0.01			ICP-MS
98-29, vent mud	Stevenson Island	3.4	-3.5	64.4	17.0	0.14	10.58	0.20	1.24	0.015	0.13			0.15			ICP-MS
98-30a, vent mud	Stevenson Island	3.4	-1.5	69.1	14.4	0.28	9.44	0.22	0.27	0.023	0.08			0.14			ICP-MS
98-30b, vent mud	Stevenson Island	3.6	-1.3	70.4	14.0	0.42	8.01	0.30	0.36	0.063	0.15			0.15			ICP-MS
98-32, vent mud	Stevenson Island	3.7	8.1	74.4	12.7	0.78	4.00	0.72	0.73	0.028	0.47			0.05			ICP-MS
98-19, vent mud	West Thumb deep vent	-3.8		71.9	16.1	0.56	2.86	1.02	1.38	0.015	0.04			0.01			ICP-MS
98-16a, vent mud	West Thumb off Grant		11.2	72.8	10.2	1.11	4.29	1.57	1.66	1.291	0.97			0.0004			ICP-MS
98-16b, vent mud	West Thumb off Grant		12.1	73.9	12.7	0.76	2.29	2.29	0.70	0.023	1.28			0.0002			ICP-MS
98-17, vent mud	West Thumb off Grant		10.8	66.7	15.7	1.96	2.86	3.01	1.36	0.045	2.29			0.0001			ICP-MS

Table 2. Major element and stable-isotope data for vent deposits and vent muds—*Continued*.

Sample number/description	Location	$\delta^{34}S$	$\delta^{18}O$	SiO_2* (wt %)	Al_2O_3 (wt %)	CaO (wt %)	$FeTO_3$ (wt %)	K_2O (wt %)	MgO (wt %)	MnO (wt %)	Na_2O (wt %)	P_2O_5 (wt %)	TiO_2 (wt %)	S (wt %)	LOI (925°C)	Total	Analytical method
WEST THUMB SEDIMENTS																	
WT core, 25–26 cm, mud	Central West Thumb			85.5	3.21	0.56	2.00	0.43	0.56	0.112	0.34	0.69	0.12	0.30			ICP-MS
WT core, 25–26 cm, mud	Central West Thumb			85.0	3.40	0.56	2.14	0.47	0.60	0.127	0.35	0.78	0.13	0.30			ICP-MS
WT core, 26–27 cm, mud	Central West Thumb			81.3	5.48	1.04	2.57	0.77	1.18	0.112	0.59	0.37	0.17	0.30			ICP-MS
WT core, 27–28 cm, mud	Central West Thumb			85.5	3.97	0.70	1.57	0.52	0.68	0.070	0.40	0.23	0.13	0.10			ICP-MS
WT core, 28–29 cm, mud	Central West Thumb			84.8	4.35	0.70	1.72	0.57	0.75	0.074	0.44	0.27	0.15	0.10			ICP-MS
WT core, 28–29 cm, mud	Central West Thumb		16.4	85.4	3.97	0.70	1.57	0.58	0.68	0.072	0.43	0.27	0.13	0.10			ICP-MS
WT core, 29–30 cm, mud	Central West Thumb			84.5	3.21	0.56	2.29	0.45	0.53	0.155	0.35	1.51	0.12	0.20			ICP-MS
WT core, 30–31 cm, mud	Central West Thumb			84.3	3.78	0.56	2.14	0.51	0.71	0.142	0.40	0.96	0.13	0.20			ICP-MS
WT core, 31-–32 cm, mud	Central West Thumb			85.6	3.59	0.56	1.72	0.52	0.58	0.098	0.39	0.55	0.13	0.10			ICP-MS
WT core, 32–33 cm, mud	Central West Thumb		17.3	85.7	3.40	0.56	1.72	0.48	0.61	0.111	0.38	0.73	0.12	0.10			ICP-MS
WT core, 33–34 cm, mud	Central West Thumb			86.0	3.40	0.56	1.72	0.48	0.65	0.071	0.38	0.27	0.12	0.20			ICP-MS
WT core, 34–35 cm, mud	Central West Thumb			84.9	3.97	0.70	1.86	0.54	0.65	0.093	0.46	0.41	0.13	0.20			ICP-MS
WT core, 35–36 cm, mud	Central West Thumb			84.6	4.35	0.70	1.86	0.59	0.71	0.074	0.47	0.27	0.17	0.10			ICP-MS

Table 2. Major element and stable-isotope data for vent deposits and vent muds—*Continued*.

Sample number/description	Location	$\delta^{34}S$	$\delta^{18}O$	SiO_2* (wt %)	Al_2O_3 (wt %)	CaO (wt %)	$FeTO_3$ (wt %)	K_2O (wt %)	MgO (wt %)	MnO (wt %)	Na_2O (wt %)	P_2O_5 (wt %)	TiO_2 (wt %)	S (wt %)	LOI (925°C)	Total	Analytical method
WEST THUMB SEDIMENTS—*Continued*																	
WT core, 35–36 cm, mud	Central West Thumb			85.0	4.16	0.70	1.72	0.59	0.66	0.074	0.46	0.27	0.15	0.10			ICP-MS
WT core, 36–37 cm, mud	Central West Thumb			85.5	3.78	0.70	1.72	0.54	0.66	0.070	0.43	0.23	0.13	0.10			ICP-MS
WT core, 37–38 cm, mud	Central West Thumb			85.7	3.78	0.56	1.72	0.51	0.70	0.067	0.40	0.23	0.13	0.10			ICP-MS
WT core, 38–39 cm, mud	Central West Thumb			86.4	3.40	0.56	1.57	0.49	0.60	0.067	0.38	0.23	0.12	0.10			ICP-MS
WT core, 39–40 cm, mud	Central West Thumb			86.2	3.40	0.56	1.57	0.47	0.53	0.080	0.38	0.37	0.12	0.20			ICP-MS
WT core, 40–41 cm, mud	Central West Thumb			85.5	3.40	0.56	1.86	0.45	0.56	0.102	0.36	0.73	0.12	0.20			ICP-MS
WT core, 41–42 cm, mud	Central West Thumb			85.1	3.21	0.56	2.14	0.46	0.53	0.129	0.36	1.05	0.12	0.20			ICP-MS
WT core, 44–45 cm, mud	Central West Thumb		15.0	86.2	2.83	0.42	2.00	0.41	0.46	0.123	0.31	0.82	0.10	0.20			ICP-MS

*SiO_2 for samples analyzed by ICP-MS is calculated by difference, assuming LOI = 6.1 wt %, the average value for measured vent deposits. Sulfur in vent muds as sulfide, done gravimetrically by CrC_{12} extraction.

ment drapes the walls and floors of the craters in Mary Bay and West Thumb basin and can be clearly seen in seismic-reflection images (Johnson and others, 2003). An excellent example is a profile across the deep hole vent field east of Stevenson Island; this vent field and other nearby vents are related to a set of northwest-trending fissures (figs. 1 and 2).

Siliceous Vent Deposits

Hydrothermal precipitates occur on the lake bottom near active hydrothermal vents and at former vent sites that are now inactive. Hydrothermal deposits, such as in Mary Bay, in West Thumb basin, and southeast and east of Stevenson Island are characterized by centimeter- to decimeter-size tubular to irregularly shaped and branching siliceous conduits once filled with thermal fluids (fig. 3). Most common are 1- to 8-cm-diameter irregular tubes that contain 0.5- to 5-cm-diameter open conduits, in some cases filled with sediment (fig. 4). Individual conduit samples are as long as 40 cm. The outer surface of many conduits consists of soft to friable clay-rich sediment mainly comprised of diatoms, plus minor quartz, albite, smectite, and illite. The diatoms are progressively recrystallized and cemented by amorphous silica toward the center of the tube, forming the dense inner wall of the conduits. The inner conduit walls are lined or clogged with amorphous silica, the colloform texture of which indicates precipitation from hydrothermal fluids (fig. 5*A*). In many samples, there are long filamentous structures suggestive of replaced or mineralized bacteria.

Hydrothermal deposits are observed in the following settings: (1) at the bottom of or perched on the walls of hydrothermal vent areas or craters, (2) sticking out of softer sediment, or (3) lying flat on the sediment surface. In one upright conduit protruding from soft(?) sediment in West Thumb basin, native sulfur occurs as thin layers within the walls and lining the open conduit (fig. 4*E*). The native sulfur most likely results from microbial oxidation of H_2S in hydrothermal fluids. Active communities of bacteria form large mats around many active hydrothermal vent areas in Yellowstone Lake, as photographically documented and sampled with the ROV (Remsen and others, 1990). The outer surface of a conduit sample from the Stevenson Island deep vent site is coated with gypsum and yellowish natrojarosite that forms when hydrothermal sulfide oxidizes within the conduit walls. Also present in small amounts are as much as 20-cm aggregates of tiny (~1 mm) open siliceous tubes, with or without interstitial sediment present. These are essentially a smaller-scaled version of the deposits described above. Similar tubes also have been found in gravelly material at shallow depths of less than a few meters in Sedge Bay, associated with ~1-mm grains of pyrite.

In Mary Bay, irregular, "blobby"-looking conduits are typically perched on the walls of explosion craters and form an irregular surface composed of small, irregular structures, which appear to protrude directly into the water from the lake floor (fig. 3*C*). Field observations suggest that these conduits are connected at depth with fractures in the underlying sediment and have formed within the soft sediment, the structure shape controlled by fluid flow and relative porosities in the sediment. The random-appearing structures were most likely formed

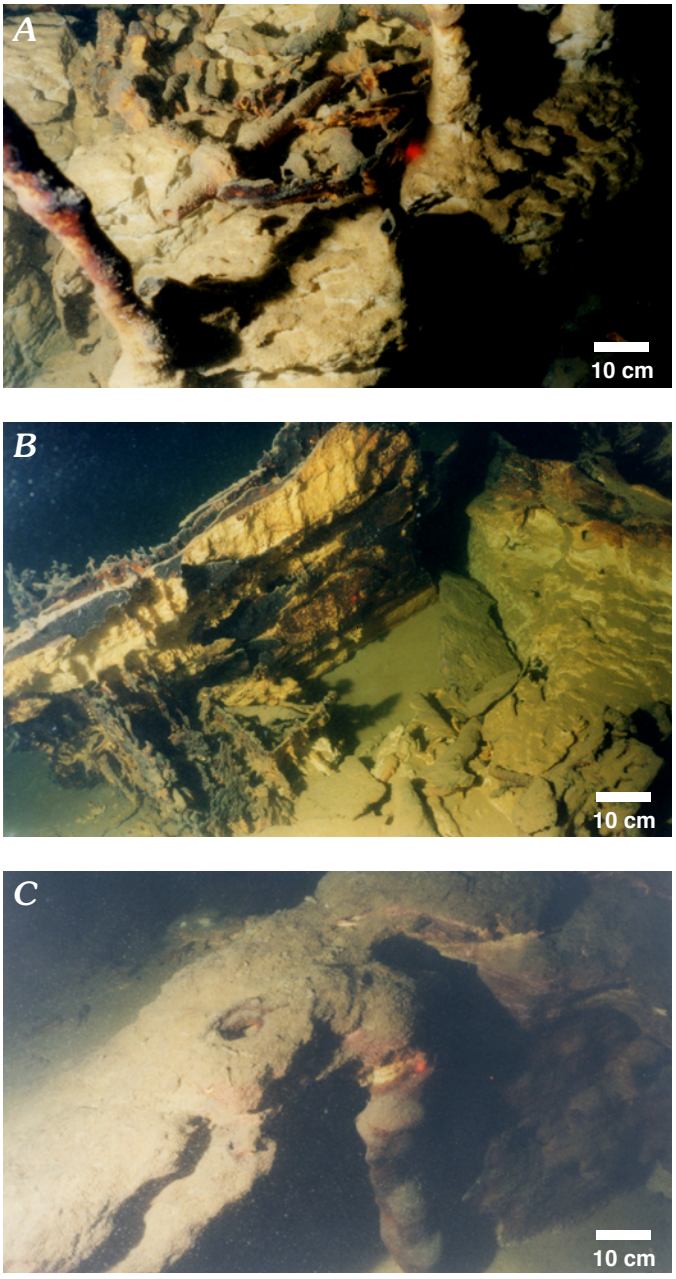

Figure 2. Lake-bottom photographs (by David Lovalvo, Eastern Oceanics, Inc.) of hydrothermal deposits from the vent area off of Grant Marina, West Thumb. All three of these areas are now exposed on the lake bottom due to sediment removal by slumping, winnowing, or dissolution. *A,* Silicified hydrothermal conduits protruding above the lake floor within vent deep. Water depth is 108 ft. *B,* Flat and branching plates of siliceous material lie on top of the sediment within deeps of West Thumb and probably formed as veins within the sediment. Water depth is 108 ft. *C,* Irregular, "blobby"-shaped conduit that terminates in surficial, flange-silicified sediments. Water depth is 73 ft.

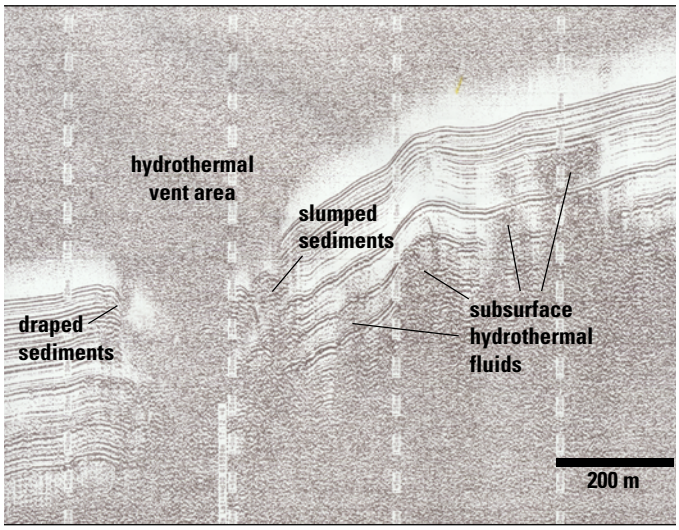

Figure 3. Seismic-reflection profile of shallow subsurface sediments at the Stevenson Island vent site.

below the sediment-water interface within sediments along conduits or vents. The structures may have been exposed later when the surrounding, unconsolidated, unaltered host sediment slumped off the harder, mineralized hydrothermal vent structure or was winnowed away by currents associated with individual vents or current dispersion on the lake floor, possibly combined and enhanced with active dissolution processes. Most of the conduit deposits are approximately 20 cm high or less. An alternative explanation for the formation of these structures is as chimneys above the sediment-water interface; however, this process is inconsistent with the horizontally layered diatomaceous sediments incorporated within the walls and onto the outside of the conduits (figs. 2 and 4). The layering and composition of these layers is very comparable to the laminated sediments found on the undisturbed lake floor.

The occurrence, morphology, and mineralogy of the siliceous conduits and tubes suggest that they formed as fluid conduits within the sediment and that the sediment between the conduits was subsequently removed, exposing the deposits at the sediment surface, where many have toppled over. Many of these conduits occur at the bottom of the vent craters, requiring a process that enables sediment to be winnowed out of 20- to 50-m-deep craters. Recent observations have noted a large (50-m diameter) sediment plume in the water column above active sets of vigorous vents in the northern basin, indicating fine-grained sediments are entrained in the hydrothermal vents during some venting processes and, if vigorous enough and sustained for a long enough time, this process might produce significant deep crater areas. In addition, geochemical studies suggest that sediment dissolution by hydrothermal fluids may be a very important process in explaining much of the detailed landscape in hydrothermal areas on the lake floor (see below).

In the West Thumb basin, irregular flat and branching horizontal plates of siliceous material, <1 cm thick by as much as tens of centimeters across, occur locally atop the sediment associated with the other hydrothermal material (figs. 2*C*, 4*D*, and 4*F*). This platy material is essentially identical to the walls of the tubes described above and may have formed as crusts on top of or veins within more permeable zones within the layered sediment (fig. 3). Lacy, fragile, network-like branching conduits (figs. 2*B* and 4*B*; table 1, sample 98-24) occur in West Thumb basin hydrothermal fields and most likely formed within sediment beneath the sediment-water interface. Joints are common in the semi-indurated sediment exposed within some craters and act as conduits for several active vents in West Thumb basin (fig. 3*B*). This process suggests that siliceous veins could be actively forming in the subsurface at these locations.

Many of the inactive siliceous conduits are stained red to dark brown as the result of coating with iron oxyhydroxides during exposure on the lake bottom, perhaps due to oxidation of hydrothermal fluids during mixing with ambient, oxygenated lake water. The iron oxides are mostly X-ray amorphous, but broad, weak peaks of goethite occur in some diffraction patterns.

Siliceous Spires

Another significant hydrothermal structure found in Yellowstone Lake consists of hard, porous siliceous material protruding vertically from crater-like depressions as irregular, conically shaped “spires” discovered in Bridge Bay in 1997. A group of 12–15 spires, as tall as 8 m with average diameters of 1–2 m, project above the diatomaceous sediment surface at a water depth of 15 m (fig. 6). Spire samples and a small (1.4 m tall), complete spire were recovered by National Park Service scuba divers in 1997 and 1999. Macroscopically, spire samples consist of white or tan, porous, punky siliceous interior with a distinctly red-brown to black outer zone. Scanning electron microscope and X-ray diffraction studies indicate that the spire deposits consist of globules of amorphous silica. The globules are about 5–10 μm in diameter (fig. 6) and form irregular aggregates, interconnecting masses, and cylinders or tubes of aggregated globules. These textures are similar to those observed for silica in active submarine hydrothermal deposits from mid-ocean ridges (Alt and others, 1987; Juniper and Fouquet, 1988). Common, tiny (~1 μm) holes in the silica are probably dissolution effects and could be microbial in origin. The overall texture suggests silica precipitation on bacterial filaments as documented in New Zealand hydrothermal systems (Jones and Renaut, 1996; Jones and others, 1997). Diatoms are sparse in the spire interiors while diatoms are abundant within spire walls, especially near the outer surface of the wall and where the spire roots extend below the sediment-water interface.

Trace amounts of smectite and quartz in the spires are probably detrital material trapped within the hydrothermal pre-

Table 3 (continued on facing page). Minor and trace-element data for vent deposits and vent muds (Ag–Hf).

[Chemical analyses by inductively coupled plasma–mass spectrometry (ICP-MS). Elements measured in parts per million]

Sample number/description	Location	Ag	As	Au	Ba	Be	Bi	Cd	Co	Cr	Cs	Cu	Ga	Ge	Hf
VENT DEPOSITS															
98-11, MB relict conduit	Mary Bay	0.31	69		840	1.4		0.08	6.0	82	37	13	10	1.5	
98-11, MB crust	Mary Bay	0.31	140		860	1.6		0.08	6.7	82	42	14	11	1.9	
94-11-2, MB bulk conduit	Mary Bay		2200		380	0.9	0.08	<0.1	3.4		36	6	<0.1	2.1	1
94-11-2, MB inner conduit	Mary Bay		3200		280	0.8	0.08	<0.1	3.2		18	10	<0.1	0.9	0.6
94-11-2, MB outer conduit	Mary Bay		440		630	1.4	0.1	<0.1	4		64	10	<0.1	2.1	2
94-12-2, MB bulk conduit	Mary Bay		310		520	1.4	0.06	0.5	6.5		28	10	<0.1	1.8	1
94-12-4, MB crust	Mary Bay		74		840	1.6	0.1	<0.1	6		38	10	<0.1	2.4	2
94-13-2, MB bulk conduit	Mary Bay		190		490	0.5	0.06	<0.1	4.1		37	6	<0.1	1.9	1
94-13-2, MB inner conduit	Mary Bay		44		220	0.5	<0.05	<0.1	1.6		28	6	<0.1	0.8	0.5
94-13-2, MB outer conduit	Mary Bay		200		440	0.5	0.05	0.6	12		50	10	<0.1	1.8	1
94-14-4, MB outer conduit	Mary Bay		380		980	2	0.1	0.2	16		46	20	<0.1	2.5	3
94-23-1, MB bulk crust	Mary Bay		330		420	0.9	0.07	0.1	5		30	8	<0.1	1.7	2
94-23-1, MB inner crust	Mary Bay		460		370	0.9	0.2	<0.1	4.6		18	20	<0.1	1	0.8
94-23-1, MB outer crust	Mary Bay	0.2	190		740	1.9	0.1	<0.1	9.4		60	10	<0.1	2.1	2
94-24-2-A, MB crust	Mary Bay	<0.1	240		640	1	0.08	<0.1	5.6		16	6	<0.1	2.5	2
94-24-2-B, MB bulk conduit	Mary Bay	<0.1	91		620	1.2	0.08	<0.1	5.4		20	8	<0.1	2	2
94-3, MB bulk conduit	Mary Bay	<0.1	83		490	0.8	<0.05	0.5	5.8		20	8	<0.1	1.8	1
94-7-1, MB crust	Mary Bay	<0.1	89		630	1.2	0.08	<0.1	5.5		21	8	<0.1	2	2
BS8, MB bulk conduit	Mary Bay	0.2	230		510	1.5	0.1	0.2	3.8		60	20	<0.1	2	2
BS8, MB inner conduit	Mary Bay	0.9	420		280	0.7	<0.05	<0.1	2.8		18	8	<0.1	0.9	0.7
BS8, MB outer conduit	Mary Bay	0.1	230		500	1.2	0.09	0.4	4.4		65	30	<0.1	1.6	2
YNP-89-SBS-11, pyritic tubes w/ sediment	Sedge Bay	0.2	5000		19	0.4	0.09	0.2	26		1.6	120	<0.1	0.4	0.9
98-29, SI sediment & pyrite veins	Stevenson Island	0.27	1000		15	0.18		0.13	42	44	0.92	50	6.6	0.33	
94-14-1, SI bulk conduit	Stevenson Island		160		750	1.4	0.1	<0.1	7.4		24	10	<0.1	1.6	2
94-14-1, SI inner conduit/crust	Stevenson Island		120		520	0.7	0.1	<0.1	4.3		14	10	<0.1	0.9	1
94-14-1, SI outer conduit	Stevenson Island		140		770	1.3	0.09	0.2	6.2		24	10	<0.1	1.3	2
94-14-4, SI bulk conduit	Stevenson Island		220		1000	1.6	0.1	<0.1	13		42	20	<0.1	3.5	3
94-14-4, SI inner conduit	Stevenson Island		95		550	1	0.06	<0.1	5		26	10	<0.1	1.1	1
98-22, WT double conduit	West Thumb deep vent	0.17	76		150	0.94		0.11	0.96	21	68	10	8.5	7.6	
98-22, WT deep vent conduit	West Thumb deep vent	0.04	1200		250	1.2		0.2	3.2	22		10	23	15	
98-23D, WT slab	West Thumb deep vent	0.08	790		47	0.45		0.04	0.38	<10	31	8.6	4.9	3.1	
98-23D, WT conduit	West Thumb deep vent	0.09	290		72	0.82		0.12	0.80	12	48	9.2	6.8	4.0	
98-24, WT relict, lacy conduit	West Thumb deep vent	0.08	930		880	4.2		0.72	23	20	25	20	16	4.4	
98-16, WT conduit	West Thumb off Grant	0.51	550		750	2.6		0.17	10	24	46	7.4	16	3.6	
98-18, WT sinter crust	West Thumb off Grant	0.18	390		270	2.4		0.27	5.2	<10	11	7.8	5.8	2.4	
98-18, WT brown slab	West Thumb off Grant	0.02	500		410	3.5		0.3	7.7	10		7	10	3.4	
BRIDGE BAY SPIRES															
97-BB1, dark outer sinter	NE Bridge Bay	0.12	28	<0.05	130	20	<0.05	0.3	2.1		2.7	5	4.8	0.6	<0.5
97-BB1, white/tan inner sinter	NE Bridge Bay	0.13	13	<0.05	330	16	0.06	<0.1	4.1		6.3	4	8.5	2.4	0.7
97-BB2, dark outer sinter	NE Bridge Bay	0.05	1700	<0.05	6600	12	<0.05	0.8	45		8.2	33	16	6.8	0.5
97-BB2, white/tan inner sinter	NE Bridge Bay	0.37	510	<0.1	59	23	<0.1	<0.2	2		2.1	<6	5.6	1	<1
WEST THUMB SINTERS															
97-WTGB-1, WT sinter	Sinter terrace WTGB	0.1	4	<0.05	5	28	0.06	<0.1	<0.1		86	<3	130	0.4	<0.5
98P94-A, WT sinter	Fishing Cone, 4 ft deep	0.08	4.9		28	71		0.02	0.24	29	200	6.9	170	0.70	0.35
98P94-B, WT sinter	Fishing Cone, 7 ft deep	0.05	5.9		30	28		0.02	0.14	<10	49	1.8	100	3.8	1.6
98P94-C, WT sinter	50m N of Fishing Cone, 4.5 ft deep	0.03	2		32	8.3		0.01	<0.1	<10	40	10	46	2.1	0.11
98P95-B, WT sinter	70 m off Fishing Cone, 14.5 ft deep	0.03	9.0		34	19		0.01	0.32	<10	69	14	170	1.1	0.43

Table 3 (continued from facing page). Minor and trace-element data for vent deposits and vent muds (Hg–Zr).

[Chemical analyses by inductively coupled plasma–mass spectrometry (ICP-MS). Elements measured in parts per million]

Hg	Li	Mo	Nb	Ni	Pb	Rb	Sb	Sc	Se	Sn	Sr	Ta	Th	Tl	U	V	W	Y	Zn	Zr
VENT DEPOSITS																				
	12	2.1		20	13	47	2.8		0.3		440	0.77	6.1	0.3	1.7	52	13		31	
	12	2.8		21	14	48	3.4		0.3		450	1.0	6.5	0.3	1.8	51	25		31	
6.1	8.9	1.7	6.8	12	6.8	31	3.3	4	<1	0.9	180	0.4	3.4	0.2	0.99	36	36	8.6	20	75
	5.6	2.2	5	11	<0.1	16	5.1	2	<1	<0.5	120	0.5	2.2	0.1	0.66	23	17	5.8	10	46
	12	2.9	9.6	12	51	52	3.2	5.4	<1	0.6	260	0.8	5	0.3	1.5	48	61	12	20	100
0.26	6.8	3.8	6.4	16	7.3	26	3.4	4	<1	0.8	260	0.4	3.4	0.2	0.91	40	30	9.3	30	70
0.55	14	1.7	6.6	22	13	44	1.9	7.2	<1	1	460	0.4	6.5	0.3	1.6	52	15	14	36	140
2.7	8.9	2	7	13	6.8	26	2.4	4	<1	0.6	180	0.4	3.4	0.2	0.97	35	58	8.4	20	68
1.6	5	1.3	4	7	1	17	1.5	2	<1	<0.5	84	0.3	1.7	0.1	0.5	18	9.9	4.5	8	34
	11	4.1	7.3	15	88	33	4.1	4	<1	<0.5	180	0.5	4.1	0.2	1.3	41	150	11	20	66
1.8	12	9.7	14	23	16	60	9.3	8.4	<1	5	430	1	7.2	0.3	1.9	83	71	17	39	140
0.68	11	2.2	9	18	7.8	26	3.1	4	<1	2	220	0.4	3.8	0.2	1.1	41	29	10	20	80
	8.7	2.1	8.3	17	7.5	20	3.4	3	<1	<0.5	200	0.5	3.2	<0.1	1.2	31	18	9.8	20	70
	17	2.8	13	23	13	45	4.8	6.7	<1	<0.5	360	0.7	6.4	0.3	1.7	60	77	16	30	120
0.48	12	1.8	6.2	19	10	32	2	6.1	<1	0.9	370	0.3	5	0.3	1.5	44	39	12	30	100
0.18	14	1.4	8.6	20	9.8	32	1.3	5.6	<1	0.8	370	0.5	4.9	0.2	1.4	39	19	11	20	100
0.95	9.7	1.5	5.4	24	5.6	26	1.4	5	<1	<0.5	280	0.2	3.4	0.4	1	27	30	7.8	20	74
0.38	14	1.4	9.1	21	10	33	1.3	5.8	<1	0.8	380	0.5	4.9	0.2	1.3	41	19	11	30	100
14	11	3.6	7.8	11	10	42	4.9	5	<1	1	210	0.5	4.3	0.2	1.2	42	23	11	20	88
55	5.9	2	4.8	11	4.4	17	2.4	2	<1	<0.5	120	0.3	2.1	0.2	0.54	21	7.9	6.2	10	43
3.1	11	2.6	8.3	13	12	45	2.3	5	<1	2	210	0.6	4.2	0.2	1.3	39	41	12	36	90
9.1	0.2	100	22	5.2	110	22	<0.05	240	4	7	5.3	6.2	<0.5	2.5	4.4	0.89	35	12	6.6	53
	0.4	35		240	27	0.32	18		2.6		3.6	0.89	3.5	1.3	1.0	40	120		45	
0.51	14	2.5	12	26	12	37	3.9	6.4	<1	1	400	0.8	5.6	0.3	1.4	57	15	14	34	120
	9.1	1.6	7.7	16	8.1	24	2.8	4	<1	0.8	250	0.6	3.7	0.1	0.96	33	8.8	8.6	20	78
	14	2.2	12	22	11	39	3.6	5.7	<1	0.7	390	1.2	5.7	0.2	1.4	53	16	13	30	120
2.2	14	8.6	15	27	16	62	7.9	9.2	<1	2	500	1.1	7.7	0.4	1.9	89	36	19	46	170
1	5.4	2.4	6.9	13	6.6	31	3.3	4	<1	0.5	220	0.5	3.3	0.1	0.9	35	14	10	20	63
	5.4	0.78		6.7	4.3	26	5.6		0.2		42	0.37	1.7	0.2	0.74	8.8	26		11	
	8.7	2.1		6.7	8.1	49	11		<1		89		3.1	0.6	1.6	32	78		10	
	1.2	3.9		3.0	2.0	12	26		<0.2		12	0.2	0.73	0.1	0.36	6.8	18		<5	
	2.3	3.0		5.9	2.9	18	5.5		0.1		17	0.2	1.1	0.2	0.79	10	51		5.5	
	8.3	17		150	4.3	18	15		0.5		67	<0.2	3.0	12	2.2	60	450		29	
	18	13		29	14	75	22		0.5		100	1.3	12	2.4	3.4	25	200		35	
	5.7	25		46	2.8	13	40		0.2		23	<0.2	1.8	5.1	0.93	15	260		11	
	13	16		70	4.3	16	18		<1		38		3.2	8	1	24	250		20	
BRIDGE BAY SPIRES																				
	6.7	1.9	8.3	16	3.6	6.3	6	1	<1	<0.5	53	<0.1	1	0.1	1.6	13	40	8.6	10	9.2
	16	1.3	7.2	16	7.2	19	5.4	2	<1	0.7	150	0.1	2.9	0.2	1.6	28	6.8	6.8	10	51
	60	57	0.5	520	5.8	22	20	3	<1	<0.5	250	<0.1	3.2	27	2.8	180	390	15	52	8.7
	4	2	19	21	5.9	4.1	14	<1	<2	<1	21	<0.2	1	<0.2	2.5	44	110	5.8	<6	18
WEST THUMB SINTERS																				
	9.4	0.2	0.2	0.4	1	13	55	<0.5	<1	<0.5	3	<0.1	<0.05	0.2	0.2	<1	4.3	0.8	<3	0.4
	5.7	0.96	<2	16	1.7	23	12	<0.3	<0.2		6.9	<0.2	0.44	0.2	0.15	<0.4	1.0	1.5	<5	
	6.0	0.23	2.1	<1	1.5	14	37	<0.3	<0.2		5.8	<0.2	0.49	0.1	0.44	1.4	3.9	1.5	<5	
	3.1	0.2	<2	<1	1.3	9.2	44	<0.3	<0.2		2.9	<0.2	0.30	0.06	0.14	1.1	3.7	0.51	<5	
	5.4	0.74	<2	1.3	1.2	12	66	<0.3	<0.2		6.4	<0.2	0.29	0.07	0.16	0.8	1.4	0.68	<5	

Table 3 (continued on facing page). Minor and trace-element data for vent deposits and vent muds (Ag–Hf)—*Continued.*

Sample number/description	Location	Ag	As	Au	Ba	Be	Bi	Cd	Co	Cr	Cs	Cu	Ga	Ge	Hf
WEST THUMB SINTERS—*Continued*															
98P96-B, WT sinter	70m/20 deg S of Fishing Cone, 18 ft deep	0.05	17		130	25		0.02	0.26	<10	49	6.8	88	3.2	3.0
VENT MUDS															
98-03, vent mud	Mary Bay	<0.02	77		1100	1.7	0.06	0.1	12	120		20	17	2.5	
98-26, vent mud	Mary Bay	0.06	140		1200	1.6	0.08	0.2	13	140		20	18	2.1	
98-27, vent mud	Mary Bay	0.06	150		600	1.6	0.1	0.1	8.6	170		20	24	1.2	
Core 3-1 (0–10cm), vent mud	Mary Bay	0.08	130		1100	1.6	0.1	0.2	11	110		20	17	2.2	
Core 3-2 (20–30cm), vent mud	Mary Bay	0.03	130		960	1.7	0.1	0.2	11	110		20	16	2.2	
Core 3-3 (40–45cm), vent mud	Mary Bay	0.06	130		1100	1.9	0.1	0.2	12	110		20	18	2.1	
98-29, vent mud	Stevenson Island	<0.02	330		99	1.7	0.2	0.2	41	120		75	36	0.7	
98-30a, vent mud	Stevenson Island	0.08	240		110	1.4	0.1	0.2	38	150		64	28	1.2	
98-30b, vent mud	Stevenson Island	0.1	340		190	1.9	0.2	0.2	39	120		56	27	2.3	
98-32, vent mud	Stevenson Island	0.1	220		370	1.8	0.1	0.2	23	110		55	24	5.6	
98-19, vent mud	West Thumb deep vent	1.1	93		230	2.8		0.07	3.6	150		20	32	1.9	
98-16a, vent mud	West Thumb off Grant	0.03	860		870	5.2	0.1	0.3	17	62		30	67	9.4	
98-16b, vent mud	West Thumb off Grant	0.04	160		710	2.6	0.2	0.1	5.8	72		20	23	10	
98-17, vent mud	West Thumb off Grant	0.08	75		1100	2.8	0.3	<0.1	15	110		20	20	2.3	
WEST THUMB SEDIMENTS															
WT core (25–26 cm), mud	Central West Thumb	0.4	430	0.001	230	3.8	0.1	0.2	7.4		13	20	<0.1	21	1
WT core (25–26 cm), mud	Central West Thumb	<0.1	480	0.002	230	3.5	0.1	0.2	7.7		13	20	<0.1	21	1
WT core (26–27 cm), mud	Central West Thumb	0.2	620	<0.0007	400	5.4	0.3	0.7	12		21	33	<0.1	21	2
WT core (27–28 cm), mud	Central West Thumb	<0.1	240	<0.0007	280	3.5	0.2	0.2	5.4		15	10	<0.1	11	1
WT core (28–29 cm), mud	Central West Thumb	<0.1	260	0.002	320	3.9	0.2	0.2	5.8		16	20	<0.1	14	2
WT core (28–29 cm), mud	Central West Thumb	<0.1	250	0.0008	290	2.9	0.2	0.2	5.5		15	20	<0.1	13	1
WT core (29–30 cm), mud	Central West Thumb	<0.1	540	0.001	260	3.2	0.2	0.2	6.6		13	20	<0.1	17	1
WT core (30–31 cm), mud	Central West Thumb	<0.1	410	0.0008	280	3.3	0.2	0.2	7.1		14	20	<0.1	16	1
WT core (31–32 cm), mud	Central West Thumb	<0.1	360	0.003	280	3.3	0.2	0.2	6.4		14	20	<0.1	15	1
WT core (32–33 cm), mud	Central West Thumb	<0.1	330	0.0009	260	3.2	0.1	0.3	6.5		13	10	<0.1	15	1
WT core (33–34 cm), mud	Central West Thumb	<0.1	320	<0.0007	260	3.4	0.2	0.2	5.9		12	20	<0.1	14	1
WT core (34–35 cm), mud	Central West Thumb	<0.1	260	<0.0007	290	3.4	0.2	0.7	6.9		13	20	<0.1	14	1
WT core (35–36 cm), mud	Central West Thumb	<0.1	300	0.003	340	4.1	0.2	0.3	6.8		14	20	<0.1	13	2
WT core (35–36 cm), mud	Central West Thumb	<0.1	300	<0.0007	310	3.1	0.2	0.2	6.6		13	20	<0.1	12	1
WT core (36–37 cm), mud	Central West Thumb	<0.1	270	<0.0007	300	3.7	0.2	0.4	6.4		13	10	<0.1	13	1
WT core (37–38 cm), mud	Central West Thumb	<0.1	240	0.002	290	4	0.2	0.2	6.6		13	10	<0.1	14	1
WT core (38–39 cm), mud	Central West Thumb	<0.1	270	0.001	270	3.5	0.1	0.2	5.7		12	20	<0.1	14	1
WT core (39–40 cm), mud	Central West Thumb	<0.1	330	0.001	260	3.8	0.2	0.2	5.7		12	10	<0.1	16	1
WT core (40–41 cm), mud	Central West Thumb	<0.1	340	0.001	260	4.4	0.2	0.4	6.1		12	10	<0.1	15	1
WT core (41–42 cm), mud	Central West Thumb	<0.1	580	0.001	260	4.5	0.2	0.4	7.8		12	20	<0.1	18	1
WT core (44–45 cm), mud	Central West Thumb	<0.1	430	0.002	230	4	0.1	0.2	6.5		10	10	<0.1	18	1

Table 3 (continued from facing page). Minor and trace-element data for vent deposits and vent muds (Hg–Zr)—*Continued.*

Hg	Li	Mo	Nb	Ni	Pb	Rb	Sb	Sc	Se	Sn	Sr	Ta	Th	Tl	U	V	W	Y	Zn	Zr
WEST THUMB SINTERS—*Continued*																				
	8.3	0.1	2.0	1.5	1.7	11	23	<0.3	<0.2		8.8	0.2	0.76	0.1	0.24	2.3	7.2	2.1	14	
VENT MUDS																				
	21	2.3		39	26	54	3.7		<1	2	490		9.1	0.4	2.3	83	16		61	
	29	3.1		45	19	58	5.2		<1	2	580		9.2	0.5	2.2	96	26		62	
	41	7		28	17	40	9.1		<1	3	240		10	0.3	2.9	120	52		41	
	29	2		35	19	57	4.7		<1	2	500		9.3	0.4	2.4	80	16		50	
	32	2		39	20	53	4.3		<1	2	500		8.2	0.4	2.2	78	16		56	
	29	2.2		37	21	67	4		<1	3	550		9.7	0.4	2.4	81	12		54	
	43	24		120	60	2.4	13		<1	3	34		5.5	0.6	3.5	170	93		77	
	73	7.8		140	39	5.6	5		<1	3	25		7.8	0.8	3.4	130	43		100	
	64	7.7		140	42	8.7	5		<1	3	45		9.1	0.6	3.5	150	70		100	
	38	14		73	29	24	9.7		<1	3	140		9	0.4	3.6	130	58		79	
16	26	5.8		11	35	50	7.6		0.6		46		24	0.5	6.5	110	140		59	
	55	15		78	17	62	63		<1	3	180		11	5.8	4	81	410		74	
	27	70		19	23	84	42		<1	5.3	190		14	0.9	5	100	95		55	
	40	1.6		26	26	110	1.9		<1	5	350		15	0.7	4.2	96	39		83	
WEST THUMB SEDIMENTS																				
1.1	12	16	4.7	35	5.5	18	44	3	<1	0.6	76	0.3	3.1	0.3	1.6	48	36	12	32	62
	12	16	4.6	36	5.2	18	44	3	<1	0.6	76	0.3	2.9	0.3	1.6	51	36	12	33	62
	20	24	7.8	69	12	30	61	5.2	1	7	130	0.5	5.1	0.5	2.6	74	56	19	66	110
2.3	15	12	5.4	28	7	21	35	4	<1	0.7	93	0.3	3.5	0.3	1.6	46	35	13	36	74
1.8	16	13	6.1	29	7.2	23	38	4	<1	0.9	100	0.4	4	0.3	1.9	50	41	14	41	83
	15	12	5.3	27	6.8	22	35	4	<1	0.7	94	0.3	3.7	0.3	1.7	47	38	13	38	74
2.1	12	19	4.8	35	5.8	18	44	3	<1	0.6	79	0.3	3.3	0.3	1.7	45	40	12	32	64
2.1	14	12	4.8	34	6.6	20	34	4	<1	0.6	92	0.2	3.6	0.3	1.8	49	38	13	33	65
2	14	13	5.2	29	6.6	20	37	3	<1	0.7	81	0.3	3.6	0.3	1.8	48	42	13	34	68
1.8	13	12	4.7	29	6.1	19	34	3	<1	0.6	79	0.2	3.2	0.3	1.8	46	39	12	32	65
1.8	13	14	5	33	6.3	19	34	3	<1	0.6	80	0.3	3.2	0.3	1.7	46	39	12	33	65
1.7	14	13	5.7	32	7.2	21	32	4	<1	0.7	96	0.3	3.6	0.3	1.7	47	38	13	36	72
1.5	15	13	6.4	33	12	23	36	4	<1	0.9	110	0.4	4.3	0.3	2	51	43	15	40	86
	14	12	5.8	31	9.8	22	33	4	<1	0.8	100	0.3	3.6	0.3	1.7	49	37	13	39	78
1.9	14	12	5.2	31	6.4	20	33	3	<1	0.7	95	0.3	3.6	0.3	1.7	46	39	13	35	72
2.1	14	12	5.3	32	6.9	19	32	3	<1	0.7	91	0.3	3.4	0.3	1.6	45	38	12	33	72
2	12	12	5	29	6.4	19	32	3	<1	0.6	81	0.3	3.3	0.3	1.7	43	39	12	34	66
2.3	12	13	4.6	28	5.7	18	35	3	<1	0.6	79	0.3	3.2	0.3	1.8	44	42	12	31	63
2.1	11	14	4.4	31	5.6	17	36	3	<1	0.5	78	0.2	3.1	0.3	1.8	47	42	12	30	63
2.4	12	14	4.5	32	5.7	17	38	3	<1	0.5	77	0.3	3.2	0.4	1.8	49	46	12	30	63
1.7	11	13	4.1	30	5	16	34	3	<1	0.6	66	0.3	2.8	0.3	1.7	43	44	11	30	55

A

D

B

E

C

F

cipitates. The reddish coating from the outer portion of the spire is goethite plus amorphous iron oxyhydroxide. Goethite peaks are broad, suggesting poorly crystalline material or very small grain size. Similar materials have been observed in seafloor iron-oxyhydroxide deposits from seamounts (Alt and others, 1987) and form in low-energy venting situations where Fe-bearing hydrothermal fluids mix with oxygenated bottom waters.

The Bridge Bay spires must have formed in place above the sediment-water interface by growth of chimney-like features from lake-bottom hydrothermal vents, similar to seafloor hydrothermal-sulfide chimneys. No currently active hydrothermal venting is associated with spires in Yellowstone Lake, and spires are only known from the Bridge Bay field. Preliminary studies using uranium-isotope disequilibria suggest the spires formed about 11 ka (Neil Sturchio, University of Illinois at Chicago, written commun., 1998), after the last glacial event when ice receded from the central Yellowstone Lake basin (~16 ka; Pierce and others, this volume). Studies of past Yellowstone Lake shorelines (Meyer and Locke, 1986; Pierce, 1997; Pierce and others, 2002) have indicated that the lake was above present level during most of the period since the last glacial event, and there is no evidence that lake level was lower than about 5 m below present lake level. Moreover, the fragile, upright spire structures could not have formed subaerially above a lowered lake level and survived submergence with the attendant wave activity and winter ice flows.

Figure 4. Photographs of vent conduit samples. *A*, Portion of silicified conduit with partly silicified buff-gray lake sediment adhering to outer walls and partly stained by Fe-oxides. Not visible is central conduit partly filled with gray amorphous silica. Top is at right. *B,* Close-up of portion of material from sample 98-24, shown in figure 4D, showing network of interconnected millimeter-size siliceous tubes stained by Fe-oxides. Sample 72198-23D from West Thumb in water depth of 165 ft. *C,* Siliceous conduit (10 × 17 cm; top at right) with main orifice at right and smaller orifices branching off the sides (top and bottom). Exposed portion of conduit (at right) is stained red-brown (dark) by Fe-oxides. Sample 98-23D from West Thumb in water depth of 165 ft. *D*, Mass of interconnected, small (~1-mm diameter) siliceous tubes with lake sediment filling interstices. Irregular 2.5-cm central conduit runs through sample, which is 22 cm high by 25 cm wide. Base of sample (bottom) is buff-colored, similar to lake sediment, whereas exposed upper portion is stained red-brown by Fe-oxides. Sample 98-24 from West Thumb in water depth of 203 ft. *E,* Portion of 4-cm-diameter conduit with 0.5- to 1.0-cm-thick silica-rich walls and ~2-cm-diameter main conduit filled with buff sediment. Sample 98-11 from Mary Bay in water depth of 137 ft. *F,* Mushroom shaped conduit, 15 cm across × 18 cm high, in metal scoop on ROV. Upper portion of sample is semi-indurated and stained red-brown by Fe-oxides, and base of sample consists of softer gray-buff sediment. Central 2.5- to 4.0-cm-diameter conduit is lined with amorphous silica and native sulfur (not visible in photo). Sample 98-21 from West Thumb in water depth of 167 ft.

Yellowstone Lake Sediments and Altered Vent Sediments

Hydrothermally altered and unaltered sediments were sampled at several sites in the lake. A 50-cm-long core from West Thumb (sample no. YNP89) provides a sample of typical unaltered sediment accumulating on the lake bottom (table 1). Unaltered lake sediment consists mainly of opal (diatoms), as well as traces of quartz, albite, smectite, and illite, and is similar to material on the outside of siliceous hydrothermal conduits described above.

Consolidated, laminated, gray sediment exposed within the walls of hydrothermal vent craters in West Thumb consists of fine-grained quartz, smectite, and chlorite, as well as traces of illite and albite (table 1). Sediment associated with outer walls of inactive silicified conduits within the craters consists of typical modern background material (mainly opal, plus minor quartz, albite, smectite, and illite).

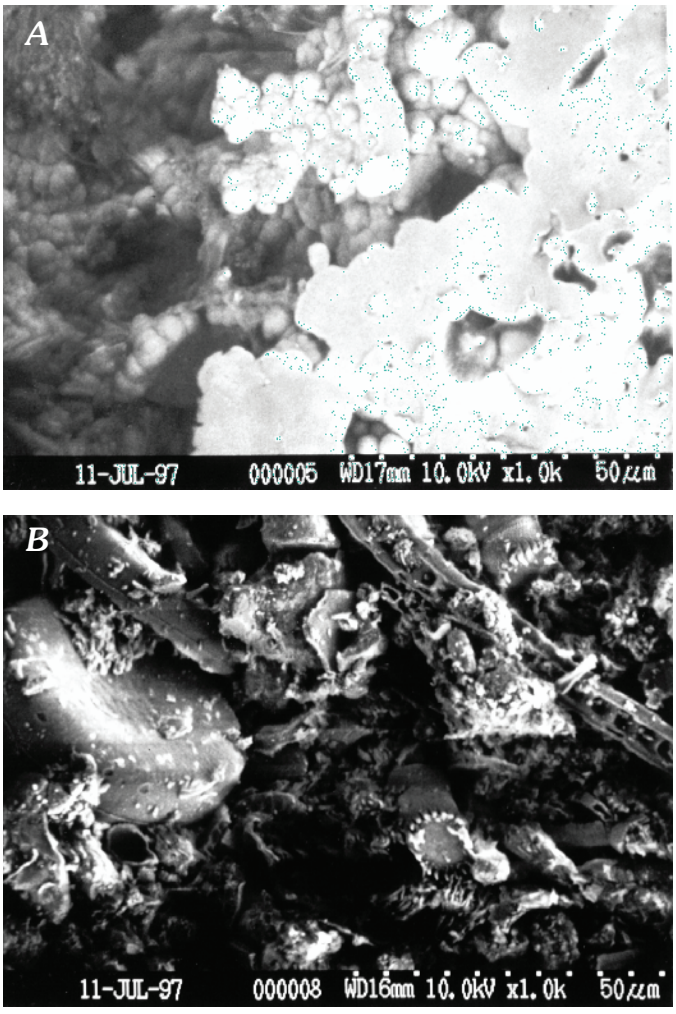

Figure 5. Scanning electron micrographs of siliceous conduit. Sample 94-11-2. *A*, Inner conduit lining consisting of amorphous silica precipitate. *B,* Outer surface of conduit with detrital material and diatoms clearly visible.

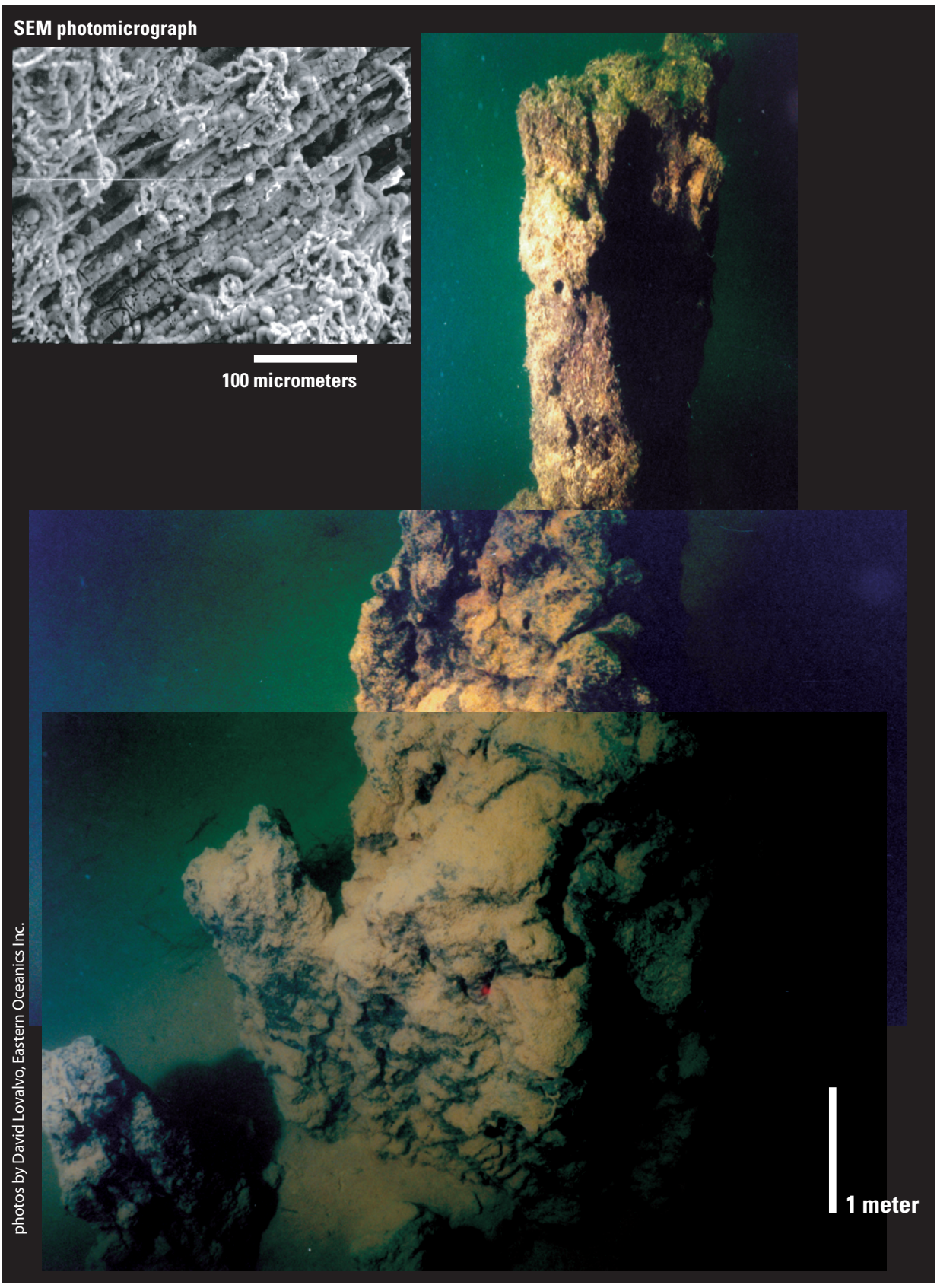

Figure 6. Underwater photomosaic of a Bridge Bay spire. Underwater photographs by David Lovalvo, Eastern Oceanics, Inc. Inset is scanning electron micrograph of siliceous spire texture.

Gray and olive-brown muds at active and inactive vents in vent craters east of Stevenson Island consist of chlorite and quartz, in addition to lesser albite, smectite, and illite. Opal in recent sediment has been recrystallized to quartz, and chlorite may be derived from hydrothermal-alteration processes. One sample of unconsolidated mud through which fluid was actively venting at a temperature of 114°C contains <1- to 2-mm blobs of native sulfur plus plates of pyrite, as much as 5 mm thick and 30 mm across.

Olive-green to black muds sampled at active 60°–120°C vents in Mary Bay by ROV and by gravity coring nearby contain quartz, albite, smectite, illite, and minor gypsum. Gypsum may have formed from oxidation of H_2S in pore waters or from oxidation of fine-grained pyrite. Opal in these sediments is completely recrystallized to quartz. There is no significant change in mineralogy along the 50-cm depth interval of the core, or between core samples and surface-sediment samples collected by ROV in this area. Altered muds in the core smelled of sulfide when sampled, and two additional cores taken nearby smelled of petroleum-like hydrocarbons. Plastic core liners used in these cores, which melt at temperatures >135°C, were partially melted and strongly deformed, reflecting high temperatures in the shallow subsurface. Boiling temperatures in Mary Bay are 140°–160°C at the depths of the Mary Bay vents, but actual measured temperatures of venting fluids are ≤120°C, suggesting hotter fluids in the very shallow subsurface. The Mary Bay hot core and a similar core from West Thumb yielded pore water with high concentrations of Cl reflecting a deep, high-temperature origin (Balistrieri and others, this volume).

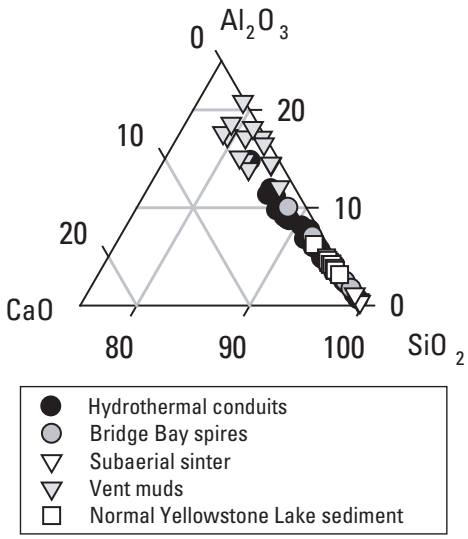

Figure 7. Ternary diagram of SiO_2-Al_2O_3-CaO for sublacustrine sinter deposits and altered and unaltered Yellowstone Lake sediments.

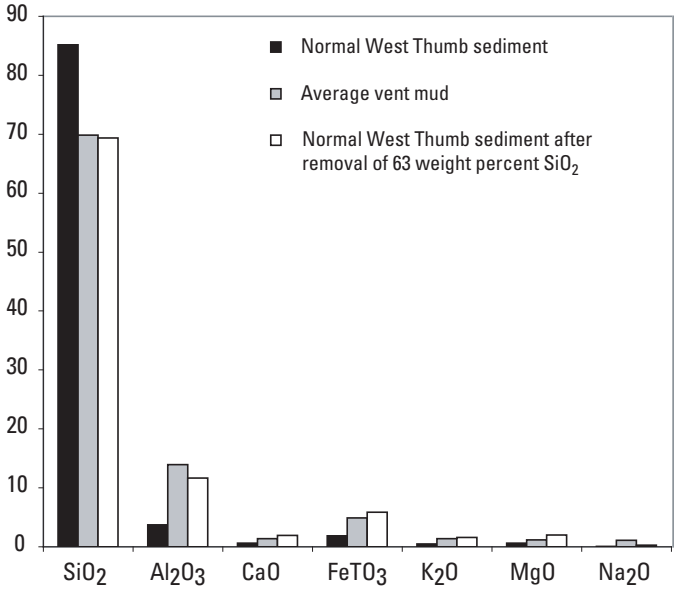

Figure 8. Plots of sediment leaching calculations showing that removal of 63 weight percent SiO_2 from average unaltered West Thumb sediment produces a sediment very close in composition to the hydrothermally altered vent muds.

Geochemistry

Major-Element Systematics

Unaltered West Thumb lake sediments (table 2) have high SiO_2 contents (81.3–86.4 weight percent), Al_2O_3 (2.8–5.5 weight percent), minor amounts of CaO, Na_2O, and K_2O (<1 percent each), low $FeTO_3$ (1.6–2.6 weight percent; $FeTO_3$ indicates total iron calculated as Fe_2O_3), and MgO (0.5–1.2 weight percent). In contrast, altered muds from hydrothermal vents have lower contents of SiO_2 and greater Al_2O_3, CaO, Na_2O, K_2O, $FeTO_3$, and MgO than the modern opal-rich background sediment. This reflects dissolution of opal and passive enrichment of other components. Dilution by hydrothermal addition of chlorite could not explain the Ca-Na-K enrichments.

Chemical variations between altered and unaltered sediments, compared with hydrothermal deposits, are illustrated on a ternary diagram of SiO_2-Al_2O_3-CaO (fig. 7). This projection shows that the altered mud samples (vent muds) are depleted in SiO_2, strongly enriched in Al_2O_3, and somewhat enriched in CaO relative to unaltered Yellowstone Lake sediment. In order to test whether these trends fit a silica dissolution model, silica removal and its affect on sediment chemistry was calculated by removing successive amounts of silica and recalculating to 100 percent. Results show that the average chemistry of the vent muds is consistent with removal of 63 weight percent SiO_2 from average unaltered West Thumb sediment (fig. 8). This calculation slightly underestimates the amount of Al_2O_3 and Na_2O in altered muds and overestimates CaO, K_2O, and MgO, especially for Stevenson Island vent muds. Also, $FeTO_3$ is quite enriched in Stevenson Island vent muds compared to the calculated values.

These results suggest that, in West Thumb and Mary Bay vent muds, silica leaching is accompanied by the addition of Na_2O and Al_2O_3. In the Stevenson Island vent field, silica leaching is accompanied by the addition of $FeTO_3$ and the

removal of CaO, K_2O, and MgO, and Na_2O. These trends are consistent with the more intense alteration observed in Stevenson Island vent muds, with abundant chlorite that must be iron-rich to account for the increased $FeTO_3$ in the altered sediment.

Could these trends be produced by physical winnowing of fine-grained sediments or is a chemical process required? Obviously, the simple calculation done here cannot differentiate between physical and chemical removal of SiO_2. However, the indicated removal of alkalis and alkaline earth elements from the Stevenson Island muds, coupled with the addition of iron to form chlorite, favors a chemical process. In addition, chemical variation in hydrothermal conduits (fig. 7), which are basically vent sediments cemented in place and silicified in the inner annulus, suggests a similar silica-leaching process. SiO_2 in conduits varies from values close to pure silica, such as subaerial sinter, to SiO_2-Al_2O_3-CaO abundances similar to vent muds. Because physical winnowing is precluded in the conduit wall, where original sedimentary layering is often preserved, we conclude that chemical-leaching processes can produce the observed chemical changes in conduit-wall sediments. Vent muds show more extreme chemical changes than conduits, which may be attributed to more intense chemical leaching or perhaps to a combination of leaching and entrainment of diatom-rich fractions of the sediment due to vent-fluid advection.

Dissolution of sediments probably is caused by heating of the sediments due to hydrothermal fluid circulation, causing dissolution of amorphous silica as solubility increases. In detail, this process is complicated and influenced by fluid composition and by the kinetics of recrystallization to quartz. Balistrieri and others (this volume) have concluded from δD-Cl systematics that sublacustrine hydrothermal fluids boil on ascent due to pressure release. Steam that separates from ascending fluids is expected to be initially silica-poor but, upon condensation associated with cooling, would equilibrate by dissolving amorphous silica. Reaction with condensed steam may be the driving mechanism causing dissolution in vent craters. Possibly, simple mixing of hydrothermal fluid with ambient pore waters may lead to silica undersaturation during sublacustrine venting.

Trace Elements in Vent Fluids and Sinter Deposits

Hydrothermal fluids in Yellowstone National Park have compositions that are strongly affected by boiling and by mixing in the shallow subsurface (Fournier, 1989). In most of the Park, hot springs deposit siliceous sinter; the exceptions are areas like Mammoth Geyser Basin where hydrothermal fluids that have reacted with Paleozoic or Mesozoic carbonates in the subsurface and deposit travertine at the surface. Hydrothermal vent fluids in Yellowstone Lake have much in common with other thermal waters in the Park, including a common source from deep thermal water that has δD values of –149 per mil and Cl of ~315 mg/L (Truesdell and others, 1977; Balistrieri and others, this volume).

Chemical analyses of sublacustrine hydrothermal vent fluids indicate that active vents in Mary Bay, Stevenson Island, and West Thumb have different compositional signatures (Gemery-Hill and others, this volume). West Thumb vent fluids are more enriched in hydrothermal-indicator elements B, As, Cs, Ge, Li, Mo, Sb, and W (Balistrieri and others, this volume) relative to vents in Mary Bay.

Chemical analyses of siliceous hydrothermal deposits (table 3; fig. 9) indicate that West Thumb deposits are enriched in As, Cs, Hg, Tl, and W. Mary Bay and Stevenson Island hydrothermal deposits are commonly enriched in Ba and Cs and depleted in Cu, Mn, Mo, and Sb with respect to normal lake sediments. Bridge Bay spire samples are enriched in As, Ba, Co, Mo, Tl, and W relative to normal Yellowstone Lake sediments. Vent muds are enriched in Ba, Co, Cs, Cu, Fe, Ni, Tl, and V and are depleted in As, Mn, Mo, and Sb suggesting a possible source for the hydrothermal-indicator elements in vent fluids and vent deposits. However, the hydrothermal-indicator elements are the same throughout the Yellowstone Plateau, suggesting that subsurface reaction with underlying rhyolitic lava flows and ignimbrites must be the major source of these elements. None of the sublacustrine sinter deposits are enriched in Au or Ag.

Stable-Isotope Systematics

Oxygen Isotopes in Siliceous Deposits and Altered Sediments

Oxygen-isotope values in sublacustrine sinter and vent-mud samples range from –3.5 to 20.3 per mil (table 2), with the lower values indicating formation at higher temperatures. Unaltered West Thumb sediments have $\delta^{18}O$ values from 15.0 to 17.3 per mil, and subaerial West Thumb sinter samples have values from 20.6 to 21.4 (table 2).

Stable isotopes of hydrogen and oxygen have been analyzed on river, creek, lake, and vent-fluid waters (Balistrieri and others, this volume; Gemery-Hill and others, this volume). The water isotopes show that vent-fluid samples have values very similar to lake waters, -16.5 ± 0.5 per mil, because they are diluted by lake water during sampling or mixing in the shallow subsurface. Recharge waters for the deep hydrothermal systems in the Park initially had $\delta^{18}O$ values of about –20 per mil, corresponding to meteoric waters with δD values of –149 per mil, which is interpreted as a mixture of glacial-age waters and present-day recharge (Rye and Truesdell, this volume). However, as the recharge waters are heated in subsurface hydrothermal systems, oxygen isotopes exchange with silicate rocks and evolve by water-rock interaction to higher $\delta^{18}O$ values. Boiling of hydrothermal fluids during ascent must also influence the

$\delta^{18}O$ values, and this process will also cause ^{18}O enrichment as isotopically light steam is lost from the system. Thus, the $\delta^{18}O$ values of end-member hydrothermal fluids cannot be directly measured in our vent-fluid samples because they are >95 percent ambient lake water. Values of Cl and δD for pore fluids from the hot cores (Balistrieri and others, this volume) suggest that hydrothermal fluids that are as much as 50 percent end-member fluid occur in the very shallow (<1.5 m) subsurface. The $\delta^{18}O$ values have not been measured on these end-member fluids, but $\delta^{18}O$ values of ascending vent fluids, prior to mixing, can be estimated using the measured $\delta^{18}O$ values of hydrothermal deposits and oxygen-isotope fractionation calculations.

Calculated oxygen-isotope fractionation temperatures, assuming reaction of amorphous silica sinter deposits with normal lake water ($\delta^{18}O = -16.5$), indicates a range from 78°C to 164°C (fig. 10). The progression of temperatures calculated (fig. 10) is generally consistent with those expected for the different environments. For example, subaerial West Thumb sinter, which forms from thin sheets of hot-spring waters flowing across the surface of the sinter terraces, must form at temperatures between boiling (94°C at the altitude of West Thumb Geyser Basin) and ambient air temperature. Our calculated temperatures are 51°–55°C based on silica-water oxygen-isotope fractionation.

Similarly, the spires must form at moderately low temperature because they occur in shallow water where the boiling point limits fluid temperature to about 115°C and because they contain abundant bacteria that cannot live at temperatures above 114°C (Jorgensen and others, 1990). Moreover, the spires stick up into the water column and would radiate heat effectively. Calculated oxygen isotope temperatures are 80°–96C°.

At the other end of the spectrum, sinter samples from Mary Bay and Stevenson Island, which occur in deep waters where the boiling temperature is 140°C or higher, give $\delta^{18}O$ temperatures from 127°C to 164°C. Thus, the oxygen-isotope fractionation temperatures for amorphous silica deposits are

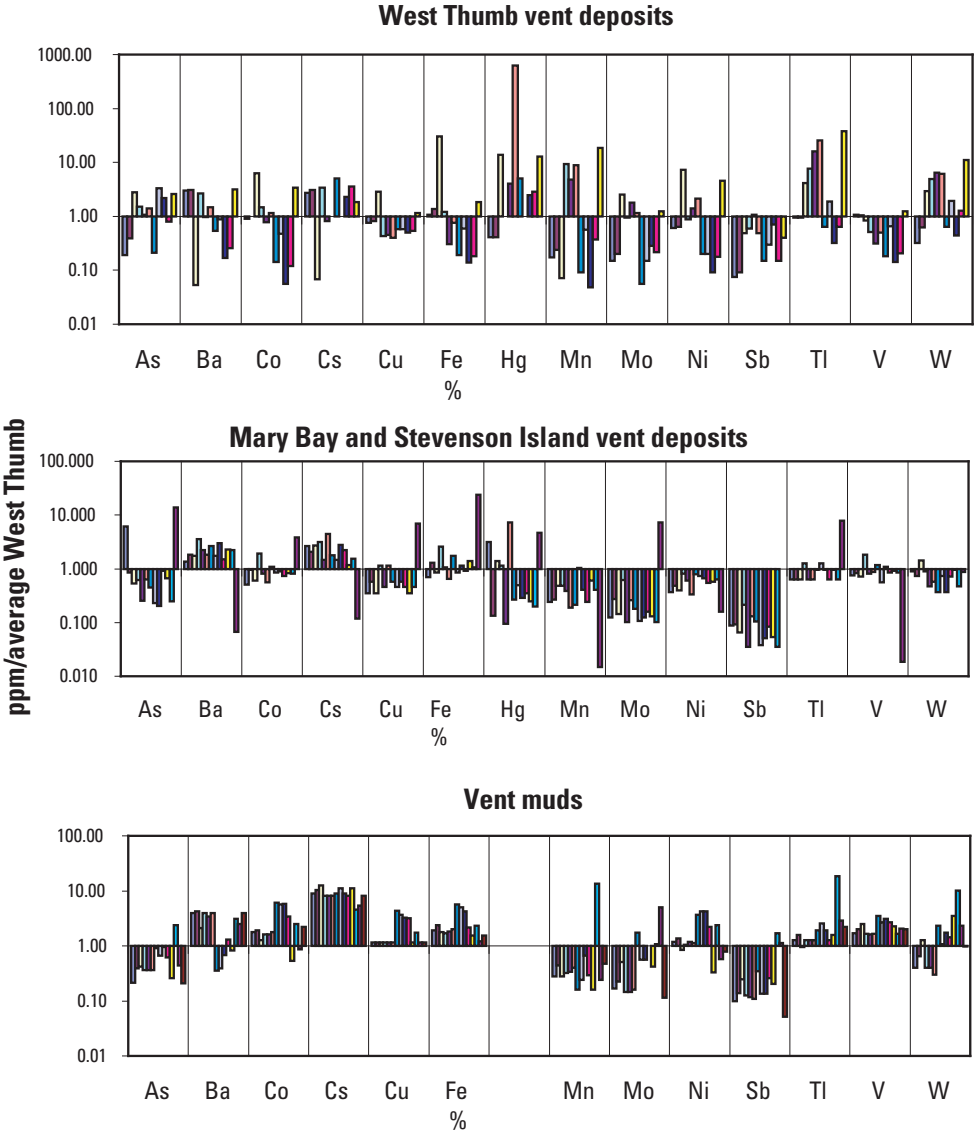

Figure 9. Enrichment-depletion diagram for trace elements in vent deposits and vent muds relative to average unaltered West Thumb sediment.

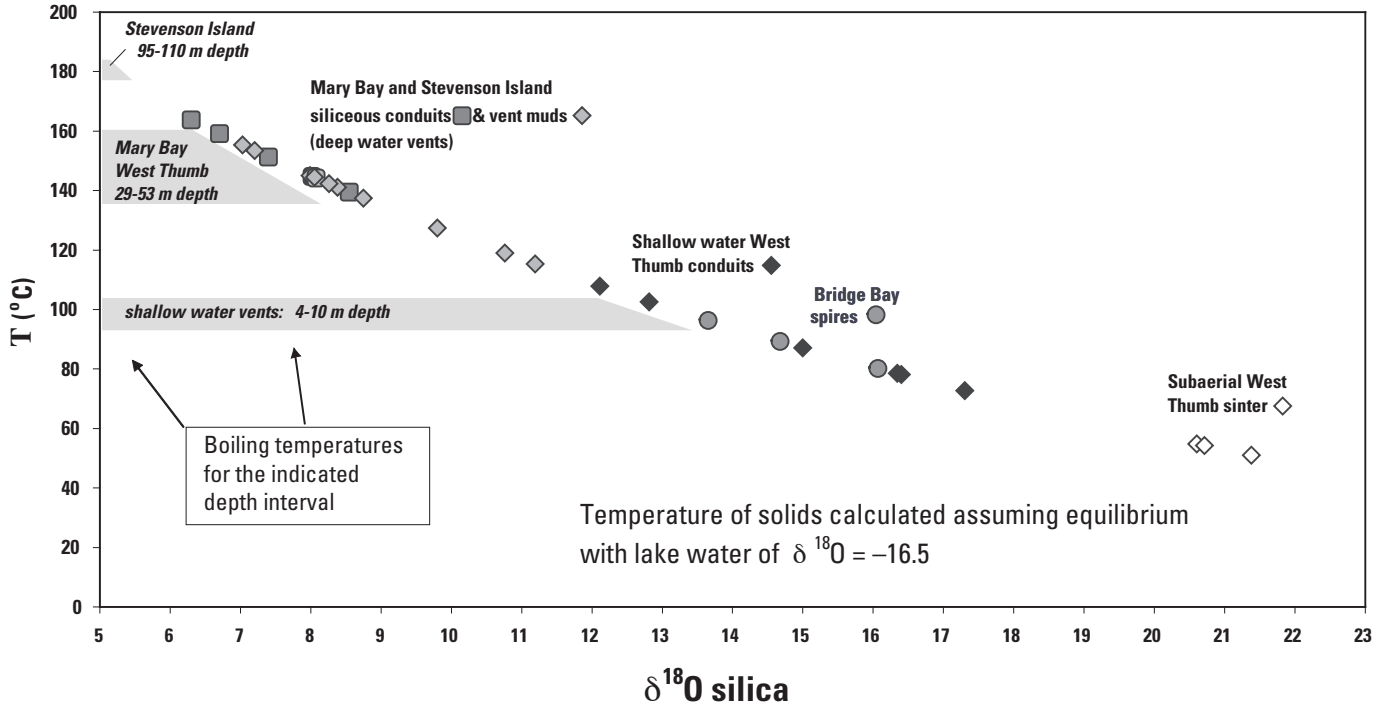

Figure 10. Plots of oxygen-isotope values of hydrothermal silica deposits versus calculated temperatures assuming formation from normal, present-day Yellowstone Lake water with $\delta^{18}O$ value of –16.5 per mil. Lake-floor boiling temperatures, which are upper limits, are noted for deposits from different depth environments.

generally consistent with geologic settings but are probably underestimated because actual vent fluids may have $\delta^{18}O$ values that are higher than –16.5 per mil (ambient lake water) due to sediment-fluid interaction on ascent.

Another approach is to estimate the $\delta^{18}O$ values of vent fluids that reacted in the shallow subsurface with silica deposits and vent muds by assuming the ascending fluids are at the boiling temperature when they reach the lake floor. This is a reasonable assumption because Cl-δD systematics (Balistrieri and others, this volume) indicate that the deep subsurface fluid beneath Yellowstone Lake is Cl rich due to boiling and has a temperature of 220°C. Calculated water $\delta^{18}O$ values, assuming vent fluids were at their boiling temperatures, range from –3.2 to –11.6 per mil (fig. 11), which are reasonable $\delta^{18}O$ values for undiluted hydrothermal fluids that have evolved to higher $\delta^{18}O$ values due to water-rock or water-sediment interaction.

Sulfur Isotopes in Lake Water, Vent Fluids, and Vent Deposits

Sulfur-isotope values of Yellowstone Lake sulfate (table 2) are quite uniform at 2.5 per mil (±0.7 per mil), suggesting that lake-water sulfate is dominated by hydrothermal sulfide. Two major sources of sulfur are possible: (1) vent sulfide that oxidizes to SO_4 in the lake (vent H_2S has measured $\delta^{34}S_{H2S}$ values of –0.5 to 3.6 per mil with an average value of 2.2 per mil) or (2) SO_4 in streams that drain into the lake. Yellowstone River and 44 tributaries that flow into Yellowstone Lake were sampled in August–September 1998; the most important streams (that is, those streams with highest flow rates and chemical fluxes) were resampled in July 1999. Sulfur-isotope analyses indicate $\delta^{34}S_{SO4}$ values range from –3.6 to 10.7 per mil with an average (not weighted for flow) of 2.6 per mil. Sufficient contrast does not exist in these data to determine whether sulfur in the lake is dominated by surface discharge into the lake or by sublacustrine hydrothermal vents. Basically, sulfur in Yellowstone Lake is dominated by volcanically derived sulfur. $\delta^{34}S$ values of sulfides in vent muds range from –3.8 to 5.7 per mil, similar to the range in stream waters.

Geochemical Model for Silica Transport and Deposition

Abundant silica deposition is unusual in hydrothermal vents on modern mid-ocean ridges, and several studies have suggested that this is because conductive cooling rather than mixing is necessary to form siliceous deposits in the subaqueous environment of the seafloor (Janecky and Seyfried, 1984; Janecky and Shanks, 1988). Moreover, high-temperature seafloor vents begin their ascent to the seafloor at quartz saturation at 350°–400°C, whereas lower

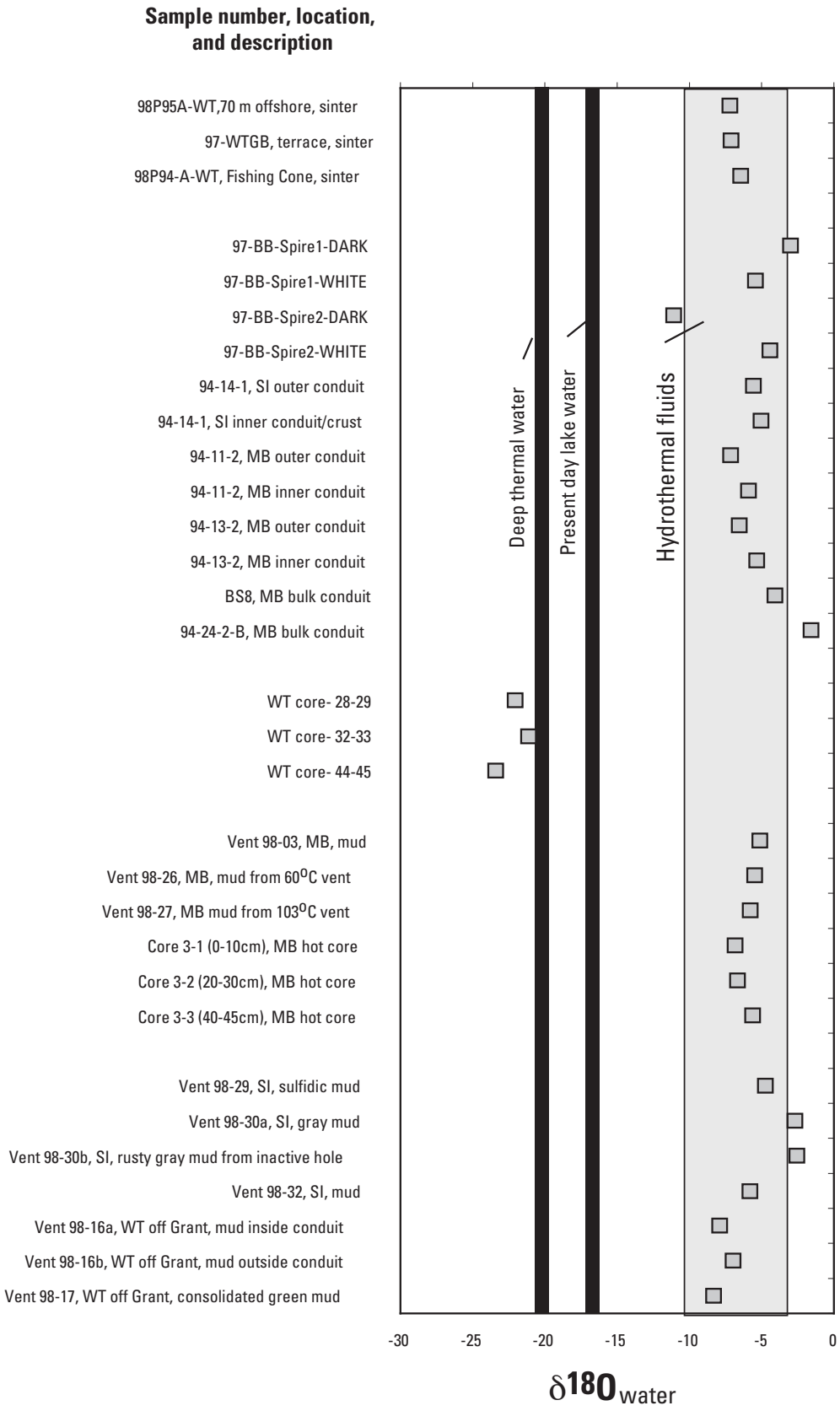

Figure 11. Oxygen-isotope composition of hydrothermal end-member fluids calculated by assuming vent fluids are in equilibrium with amorphous silica at boiling temperatures on the lake bottom when the vent deposits or vent muds formed. This approach gives a range of $\delta^{18}O$ values from –2.3 to –11.6 per mil.

temperature fluids ascending through rhyolitic glass and diatomaceous sediments beneath Yellowstone Lake may be at the much higher silica concentrations required for amorphous silica saturation.

The Yellowstone Lake silica spires are mainly amorphous silica and they apparently grew as "chimneys" above lake-bottom hydrothermal vents, based on geological arguments. In order to determine reaction and transport processes, geochemical modeling was carried out using the Geochemist's WorkBench™ incremental reaction modeling code developed by Craig Bethke and associates at the University of Illinois (Bethke, 1994).

The silica-reaction model was set up to simulate saturation of ascending solutions with amorphous silica. This was accomplished by suppressing precipitation of less soluble silica phases such as quartz, chalcedony, cristobalite, and coesite (fig. 12*A*). Precipitation of amorphous silica due to advective mixing/cooling by dilution or due to conductive cooling within the spire was tested in additional reaction models using the amorphous silica-saturated solution.

Results of these calculations (fig. 12*B*) indicate that precipitation during advective mixing of cold lake water occurs if fluids vent at temperatures >145°C. Returning to the analogy with seafloor "black smoker" sulfide chimneys, precipitation of anhydrite due to advective mixing is the initial reaction that establishes a $CaSO_4$ carapace and allows intitial chimney growth (Haymon, 1983; Styrt and others, 1981; Tivey and others, 1995). The anhydrite shell forms the leading edge of chimney growth that protects the venting hydrothermal fluid from extreme dilution due to mixing with cold bottom waters. This allows sulfide minerals to precipitate due to conductive cooling inside the chimney wall.

Similar advective mixing and amorphous silica precipitation could serve the same function in the growth of silica spires in Yellowstone Lake. Once a carapace is established, conductive cooling (without dilution) precipitates approximately 40 times as much silica sinter as advective mixing (fig. 12*C*). However, the spires occur in approximately 15-m water depth, which is too shallow due to boiling constraints for the 145°C temperature required for silica precipitation during mixing. A boiling temperature of 145°C requires about 32-m water depth, and there is no evidence that water at this site was 17 m deeper 11 ky ago (Pierce and others, this volume). Alternatively, thermophilic bacteria living at sublacustrine vent sites may have provided a protected site for silica precipitation at lower temperatures at the lake bottom. Whatever the mechanism for initially generating the spire walls, silicified bacterial filaments appear to be important in the process, and conductive cooling of vent fluids probably accounted for most of the silica precipitation.

Results of the chemical reaction modeling and other observations, as applied to spire growth, are conceptually summarized in figure 13. Oxygen-isotope analyses of silica deposits in spires indicate formation at temperatures between 80°C and 96°C. Hydrothermal circulation beneath the lake floor brings ascending hot fluids in contact with volcanic glass and with diatom-rich lake sediments. Subsurface fluid

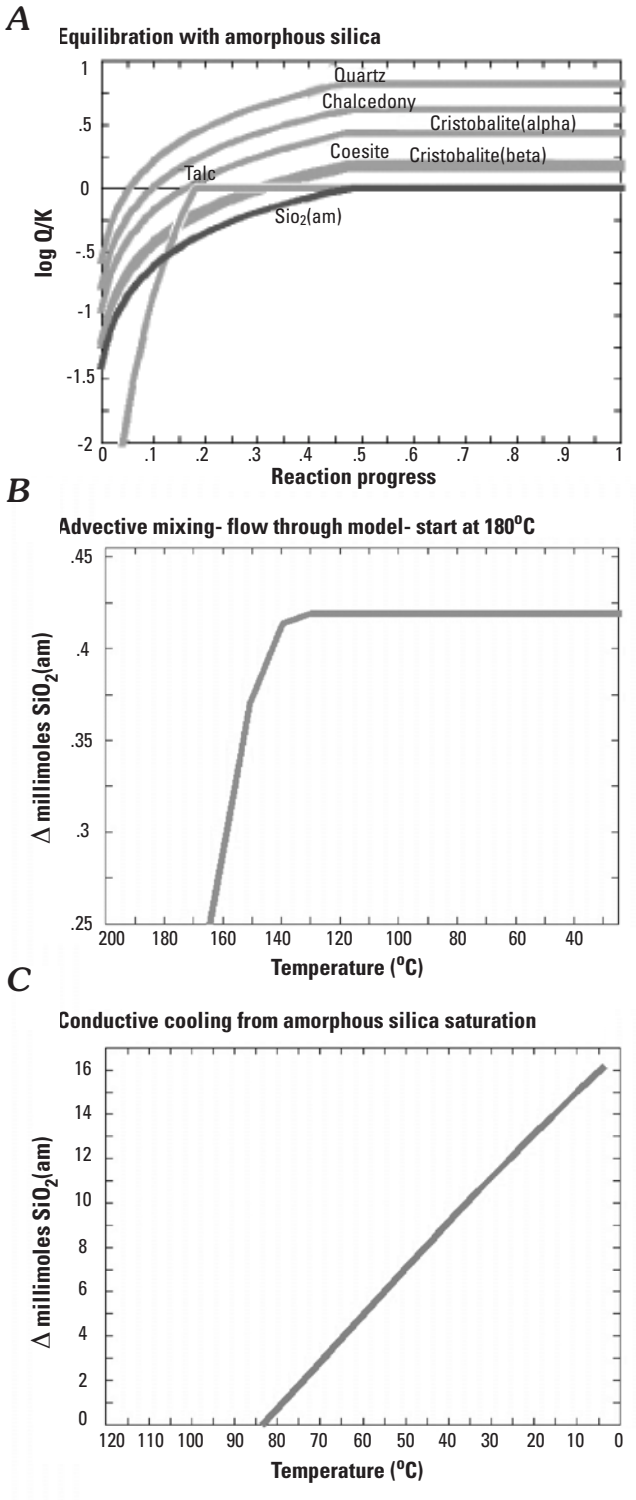

Figure 12. Incremental reaction models for: *A,* Equilibration of hydrothermal fluid with amorphous silica. *B,* Silica precipitation by advective mixing. *C,* Silica precipitation by conductive cooling.

reactions with these solids at temperatures to as much as 220°C, as indicated by vent fluid δD-Cl studies (Balistrieri and others, this volume), brings the hot fluids to saturation with amorphous silica. When these silica-rich fluids vent on the lake floor, mixing with silica-depleted, cold lake water results in precipitation of amorphous silica (fig. 13). This initial stage of spire formation produces an outer siliceous, solid shell around the vent orifice. Thus, amorphous silica precipitation is necessary to form the outer carapace of the spire and initiate spire growth. Once the shell is established, additional vent fluids traveling up the central portion of the structure can be cooled by conductive heat loss, without significant dilution due to mixing, resulting in even more rapid silica precipitation and upward growth of spires from the lake bottom.

Diatoms entrained from surficial sediments and (or) diatoms settling out of the water column, perhaps stimulated by advection of silica-rich vent fluids, are incorporated into the growing spire walls. Similarly, thermophilic bacteria that thrive in the sublacustrine vent environment are replaced and encrusted by silica as the spires grow upward from the lake floor. Bacteria are probably very important in establishing the structure that allows silicification and spire growth, but the process is not yet fully understood. It is unlikely that bacteria at the vent site have a chemical effect on the vent fluids, but sublacustrine bacterial masses and their eventual silicification may be a critical element of spire development. Perhaps bacterial mats or encrustations on the outer walls of growing spires protect vent fluids from mixing with cold dilute waters, leading to efficient silica precipitation by conductive cooling.

Why do large spires occur in shallow (15 m) water near Bridge Bay and not elsewhere in the lake? Relevant observations are (1) high resolution bathymetric mapping (Morgan and others, 2003) shows conclusively that large spires occur only in the Bridge Bay spire field, (2) spires contain abundant silicified filamentous masses (fig. 6), (3) chemical and isotopic studies indicate that spires are hydrothermal, (4) geological reasoning indicates that spires formed in-place on the lake bottom in shallow water, and (5) there are many presently active hydrothermal vents on the floor of Yellowstone Lake and some of these are in shallow-water settings similar to the Bridge Bay spire field. Observations of the silica-encased filamentous textures suggest the original thermophilic bacteria may have been cyanobacteria, which have an upper temperature limit of 73°C and are photosynthetic. We speculate that the spires require a site shallow enough to be in the photic zone so cyanobacteria can flourish around the periphery of the vents. In order to carry and deposit abundant silica, the spires must form from hot water (not steam or gas) vents. This may be a rare combination because most shallow-water vents are very gas-rich and therefore are poor transporters of silica.

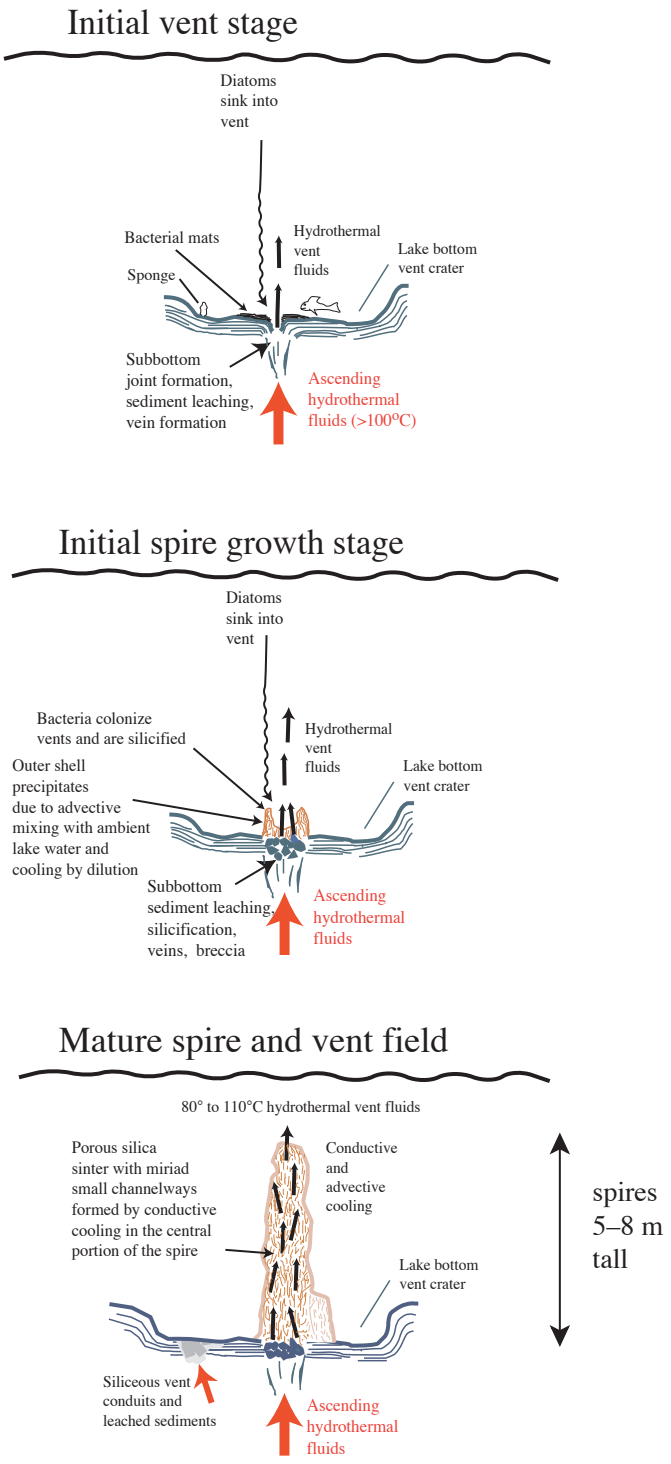

Figure 13. Schematic diagram of spire growth based on geological and geochemical observations and results of incremental reaction modeling.

Summary and Conclusions

Sublacustrine hydrothermal deposits in Yellowstone Lake are an interesting analog to ancient high-level epithermal systems. Hydrothermal elements As, Cs, Hg, Mo, Sb, Tl, and W are concentrated in the deposits but Au and Ag are not. Studies of δD and Cl in vent fluids and pore waters (Balistrieri and others, this volume) conclude that the hydrothermal fluids in Yellowstone Lake are derived from deep thermal water with about 315 mg/L Cl and are boiled on ascent to a temperature of 220°C and a Cl concentration of ~570 mg/L. This ascending fluid is mixed with lake water as it approaches and then vents on the lake floor. Boiling and mixing likely removed much of the H_2S from the ascending fluids leading to precipitation of Au at depth as sulfide-complexing breaks down.

Hydrothermal vent processes lead to development of siliceous conduits in the shallow subsurface. These pipelike features are typically filled with amorphous silica and have an outer zone that is poorly to densely silicified lake sediments. Later removal of surficial sediments by slumping or currents exposes conduit deposits in active or inactive vent fields. Vent conduits form at temperatures between 78°C and 164°C, based on oxygen-isotope geothermometry, and are limited by sublacustrine boiling temperatures at individual vent depths.

In Bridge Bay, remarkable large siliceous spires grow upward from the lake floor to heights of 8 m in water depths of 15 m. Twelve to fifteen spires are estimated to occur in Bridge Bay, and spires are unknown in other localities in the lake. Spires form at ~80°–96°C based on oxygen-isotope geothermometry, and silica deposition is caused by cooling of vent fluids initially by mixing with bottom waters and later by conductive cooling within the growing spire. Much of the spire interior appears to be silicified bacteria, suggesting that thermophilic bacteria are important in spire growth.

Hydrothermal vents in Yellowstone Lake almost invariably occur in craters on the lake bottom. These vent craters are most likely formed by sediment dissolution by vent fluids and (or) sediment entrainment and physical winnowing by vent fluids. Chemical mass-balance calculations that compare vent muds with unaltered lake sediments indicate removal of 63 weight percent SiO_2 accompanied by variable, but minor, addition or removal of the other major elements.

References Cited

Alt, J.C., Lonsdale, P., Haymon, R., and Muehlenbachs, K., 1987, Hydrothermal sulfide and oxide deposits on seamounts near 21°N., East Pacific Rise: Geological Society of America Bulletin, v. 98, p. 157–168.

Armstrong, R.L., Leeman, W.P., and Malde, H.E., 1975, K-Ar dating, Quaternary and Neogene volcanic rocks of the Snake River Plain, Idaho: American Journal of Science, v. 275, no. 3, p. 225–251.

Bacon, C.R., Gardner, J.V., Mayer, L.A., Buktenica, M.W., Dartnell, P., Ramsey, D.W., and Robinson, J.E., 2002, Morphology, volcanism, and mass wasting in Crater Lake, Oregon: Geological Society of America Bulletin, v. 114, no. 6, p. 675–692.

Bethke, C.M., 1994, The geochemist's workbench™, version 2.0—A user's guide to Rxn, Act2, React, and Gtplot: Champagne-Urbana, University of Illinois, Hydrogeology Program.

Bonnichsen, B., 1982, The Bruneau-Jarbidge eruptive center, southwestern Idaho: Idaho Bureau of Mines and Geology Bulletin , v. 26, p. 237–254.

Browne, P.R.L., and Lawless, J.V., 2001, Characteristics of hydrothermal eruptions, with examples from New Zealand and elsewhere: Earth-Science Reviews, v. 52, p. 299–331.

Christiansen, R.L., 1984, Yellowstone magmatic evolution—It's bearing on understanding large-volume explosive volcanism, *in* Explosive volcanism—Inception, evolution, and hazards: National Academy Press, p. 84–95.

Christiansen, R.L., 2001, The Quaternary and Pliocene Yellowstone Plateau volcanic field of Wyoming, Idaho, and Montana: U.S. Geological Survey Professional Paper 729-G, 145 p.

Christiansen, R.L., Foulger, G.R., and Evans, J.R., 2002, Upper-mantle origin of the Yellowstone hotspot: Geological Society of America Bulletin, v. 114, p. 1,245–1,256.

Clayton, R.N., and Mayeda, T.K., 1963, The use of bromine pentafluoride in the extraction of oxygen in oxides and silicates for isotopic analysis: Geochimica Cosmochimica Acta, v. 27, p. 43–52.

Coplen, T.B., 1995, Discontinuance of SMOW and PDB: Nature (London), v. 375, p. 285.

Cunneen, R., and Sillitoe, R.H., 1989, Paleozoic hot spring sinter in the Drummond Basin, Queensland, Australia: Economic Geology, v. 84, p 135–142.

de Ronde, C.E.J., Stoffers, P., Garbe-Schonberg, D., Christenson, B.W., Jones, B., Manconi, R., Browne, P.R.L., Hissmann, K., Botz, R., Davy, B.W., Schmitt, M., and Battershill, C.N., 2002, Discovery of active hydrothermal venting in Lake Taupo, New Zealand: Journal of Volcanology and Geothermal Research, v. 115, p. 257–275.

Ebert, S.W., and Rye, R.O., 1997, Secondary precious metal enrichment by steam-heated fluids in the Crowfoot-Lewis hot spring gold-silver deposit and relation to paleoclimate: Economic Geology, v. 92, p. 578–600.

Felicetti, L.A., Schwartz, C.C., Rye, R.O., Gunther, K.A., Crock, J.G., Haroldson, M.A., Waits, L., and Robbins, C.T., 2004, Use of naturally occurring mercury to determine the importance of cutthroat trout to Yellowstone grizzly bears: Canadian Journal of Zoology, v. 82, p. 493–501.

Fournier, R.O., 1989, Geochemistry and dynamics of the Yellowstone National Park hydrothermal system: Annual Review of Earth and Planetary Sciences, v. 17, p. 13–53.

Fournier, R.O., 1999, Hydrothermal processes related to movement of fluid from plastic into brittle rock in the magmatic-epithermal environment: Economic Geology, v. 94, p. 1,193–1,212.

Giesemann, A., Jager, H.-J., Norman, A.L., Krouse, H.R., and Brand, W.A., 1994, On-line sulfur-isotope determination using an elemental analyzer coupled to a mass spectrometer: Analytical Chemistry, v. 66, p. 2,816–2,819.

Hayden, F.V., 1878, Survey of the territories—A report of progress of the exploration in Wyoming and Idaho for the year 1878. Part II. Yellowstone National Park; geology-thermal springs-topography: U.S. Geological and Geographical Survey, Twelfth Annual Report, 503 p.

Haymon, R.M., 1983, Growth history of hydrothermal black smoker chimneys: Nature, v. 301, p. 695–698.

Hughes, S.S., and McCurry, M., 2002, Bulk major and trace element evidence for a time-space evolution of Snake River Plain rhyolites, Idaho, *in* Bonnichsen, B., White, C.M., and McCurry, M., eds., Tectonic and magmatic evolution of the Snake River Plain volcanic province: Idaho Geological Survey Bulletin 30, p. 161–176.

Humphreys, E.D., Dueker, K.G., Schutt, D.L., and Smith, R.B., 2000, Beneath Yellowstone; evaluating plume and nonplume models using teleseismic images of the upper mantle: GSA Today, v. 10, no. 12, p. 1–7.

Janecky, D.R., and Seyfried, W.E., Jr., 1984, Formation of massive sulfide deposits on oceanic ridge crests—Incremental reaction models for mixing between hydrothermal solutions and seawater: Geochimica Cosmochimica Acta, v. 48, p. 2,723–2,738.

Janecky, D.R., and Shanks, W.C., III, 1988, Computational modeling of chemical and sulfur isotopic reaction processes in seafloor hydrothermal systems—Chimneys, mounds, and subjacent alteration zones: Canadian Mineralogist, v. 26, p. 805–825.

Johnson, S.Y., Stephenson, W.J., Morgan, L.A., Shanks, W.C., III, and Pierce, K.L., 2003, Hydrothermal and tectonic activity in northern Yellowstone Lake, Wyoming: Geological Society of America Bulletin, v. 115, p. 954–971.

Jones, B., and Renaut, R.W., 1996, Influence of thermophilic bacteria on calcite and silica precipitation in hot springs with water temperatures above 90° C; evidence from Kenya and New Zealand: Canadian Journal of Earth Science, v. 33, no. 1, p. 72–83.

Jones, B., Renaut, R.W., and Rosen, M.R., 1997, Biogenicity of silica precipitation around geysers and hot-spring vents, North Island, New Zealand: Journal of Sedimentary Research, v. 67, no. 1, p. 88–104.

Jorgensen, B.B., Zawacki, L.X., and Jannasch, H.W., 1990, Thermophilic bacterial sulfate reduction in deep-sea sediments at the Guaymas Basin hydrothermal vent site (Gulf of California): Deep-Sea Research, Part A—Oceanographic Research Papers, v. 37, no. 4(A), p. 695–710.

Juniper, S.K., and Fouquet, Y., 1988, Filamentous iron-silica deposits from modern and ancient hydrothermal sites: Canadian Mineralogist, v. 26, p. 859–869.

Kaplinski, M.A., 1991, Geomorphology and geology of Yellowstone Lake, Yellowstone National Park, Wyoming: Flagstaff, Northern Arizona University, M.S. thesis, 82 p.

Kellogg, K.S., Harlan, S.S., Mehnert, H.H., Snee, L.W., Pierce, K.L., Hackett, W.R., and Rogers, D.W., 1994, Major 10.2-Ma rhyolitic volcanism in the eastern Snake River Plain, Idaho—Isotopic age and stratigraphic setting of the Arbon Valley Tuff Member of the Starlight Formation: U.S. Geological Survey Bulletin 2091, 18 p.

Klump, J.V., Remsen, C.C., and Kaster, J.L., 1988, The presence and potential impact of geothermal activity on the chemistry and biology of Yellowstone Lake, Wyoming, *in* DeLuca, M., and Babb, I., eds., Global venting, midwater and benthic ecological processes: NOAA Symposium on Undersea Research, p. 81–98.

Leeman, W.P., 1982, Rhyolites of the Snake River Plain-Yellowstone Plateau Province, Idaho and Wyoming; a summary of petrogenetic models: Idaho Bureau of Mines and Geology Bulletin, v. 26, p. 203–212.

Meyer, G.A., and Locke, W.W., 1986, Origin and deformation of Holocene shoreline terraces, Yellowstone Lake, Wyoming: Geology, v. 14, no. 8, p. 699–702.

Miller, D.S., and Smith, R.B., 1999, P and S velocity structure of the Yellowstone volcanic field from local earthquake and controlled-source tomography: Journal of Geophysical Research, v. 104, no. 7, p. 15,105–15,121.

Morgan, L.A., 1992, Stratigraphic relations and paleomagnetic and geochemical correlations of ignimbrites of the Heise volcanic field, eastern Snake River Plain, eastern Idaho and western Wyoming, *in* Link, P.K., Kuntz, M.A., and Platt, L.B., eds., Regional geology of eastern Idaho and western Wyoming: Geological Society of America Memoir 179, p. 215–226.

Morgan, L.A., Doherty, D.J., and Leeman, W.P., 1984, Ignimbrites of the eastern Snake River Plain; evidence for major caldera-forming eruptions: Journal of Geophysical Research, v. 89, no. 10, p. 8,665–8,678.

Morgan, L.A., Shanks, W.C., III, Lovalvo, D., Johnson, S.Y., Stephenson, W., Pierce, K.L., Harlan, S., Finn, C., Lee, G., Webring, M., Schulze, B., Duhn, J., Sweeney, R., and Balistrieri, L., 2003, Exploration and discovery in Yellowstone Lake—Results from high-resolution sonar imaging, seismic reflection profiling, and submersible studies: Journal of Volcanology and Geothermal Research, v. 122, p. 221–242.

Morgan, L.A., Shanks, W.C., III, Pierce, K.L., and Rye, R.O., 1998, Hydrothermal explosion deposits in Yellowstone National Park—Links to hydrothermal processes [abs.]: Eos, Transactions of the American Geophysical Union, Fall Annual Meeting, v. 79, p. F964.

Morgan, P., Blackwell, D.D., Spafford, R.E., and Smith, R.B., 1977, Heat flow measurements in Yellowstone Lake and the thermal structure of the Yellowstone caldera: Journal of Geophysical Research, v. 82, p. 3,719–3,732.

Muffler, L.J.P., White, D.E., and Truesdell, A.H., 1971, Hydrothermal explosion craters in Yellowstone National Park: Geological Society of America Bulletin, v. 82, p. 723–740.

Obradovich, J.D., 1992, Geochronology of the late Cenozoic volcanism of Yellowstone National Park and adjoining areas, Wyoming and Idaho: Open-File Report 92-408, 45 p.

Otis, R.M., 1975, Interpretation and digital processing of seismic reflection and refraction data from Yellowstone Lake, Wyoming: Salt Lake City, University of Utah, Ph.D. dissertation, 223 p.

Otis, R.M., Smith, R.B., and Wold, R.J., 1977, Geophysical surveys of Yellowstone Lake, Wyoming: Journal of Geophysical Research, v. 82, p. 3,705–3,717.

Perkins, M.E., and Nash, B.P., 2002, Explosive silicic volcanism of the Yellowstone hotspot; the ash fall tuff record: Geological Society of America Bulletin, v. 114, no. 3, p. 367–381.

Pierce, K.L., 1997, Yellowstone caldera "heavy breathing" based on Yellowstone Lake and River changes in post-glacial time: Eos, Transactions of the American Geophysical Union, v. 78, p. F802.

Pierce, K.L., Cannon, K.P., Meyer, G.A., Trebesch, M.J., and Watts, R., 2002, Post-glacial inflation-deflation cycles, tilting, and faulting in the Yellowstone caldera based on Yellowstone Lake shorelines: U.S. Geological Survey Open-File Report 02-142, 62 p.

Pierce, K.L., and Morgan, L.A., 1992, The track of the Yellowstone hot spot; volcanism, faulting, and uplift, *in* Link, P.K., Kuntz, M.A., and Platt, L.B., eds., Regional geology of eastern Idaho and western Wyoming: Geological Society of America Memoir 179, p. 1–53.

Remsen, C.C., Klump, J.V., Kaster, J.L., Paddock, R., Anderson, P., and Maki, J.S., 1990, Hydrothermal springs and gas fumaroles in Yellowstone Lake, Yellowstone National Park, Wyoming: National Geographic Research, v. 6, p. 509–515.

Smith, R.B., and Braile, L.W., 1994, The Yellowstone hotspot: Journal of Volcanology and Geothermal Research, v. 61, p. 121–187.

Styrt, M.M., Brackmann, A.J., Holland, H.D., Clark, B.C., Pisutha-Arnond, V., Eldridge, C.S., and Ohmoto, H., 1981, The mineralogy and the isotopic composition of sulfur in hydrothermal sulfide/sulfate deposits on the East Pacific Rise, 21°N. latitude: Earth and Planetary Science Letters, v. 53, no. 3, p. 382–390.

Tivey, M.K., 1995, Modeling chimney growth and associated fluid flow at seafloor hydrothermal vent sites, *in* Humphris, S.E., Zierenberg, R.A., Mullineaux, L.S., and Thomson, R.E., eds., Seafloor hydrothermal systems; physical, chemical, biological, and geological interactions: Third RIDGE Theoretical Institute, American Geophysical Union Monograph, v. 91, p. 158–177.

Truesdell, A.H., Nathenson, M., and Rye, R.O., 1977, The effects of subsurface boiling and dilution on the isotopic compositions of Yellowstone thermal waters: Journal of Geophysical Research, v. 82, no. 26, p. 3,694–3,704.

Wold, R.J., Mayhew, M.A., and Smith, R.B., 1977, Bathymetric and geophysical evidence for a hydrothermal explosion crater in Mary Bay, Yellowstone Lake, Wyoming: Journal of Geophysical Research, v. 82, no. 26, p. 3,733–3,738.